RF Project 3211 A1
Final Report

THE OHIO STATE UNIVERSITY

RESEARCH FOUNDATION

1314 KINNEAR ROAD COLUMBUS, OHIO 43212

TEMPERATURE MEASUREMENTS BEHIND REFLECTED SHOCK WAVES IN AIR

Jon B. Bader, Robert M. Nerem
Jonathan B. Dann, Michael A. Culp

Department of Aeronautical and Astronautical Engineering

7 September 1972

National Aeronautical and Space Administration
Langley Research Center
Hampton, Virginia 23365

Grant No. NGR-36-008-163

NASA CR- 132398

RF Project 3211 A1

Report No. Final

FINAL

REPORT

By

THE OHIO STATE UNIVERSITY
RESEARCH FOUNDATION

1314 KINNEAR RD.
COLUMBUS, OHIO 43212

To NATIONAL AERONAUTICAL AND SPACE ADMINISTRATION

Langley Research Center

Hampton, Virginia 23365
Grant No. NGR-36-008-163

On TEMPERATURE MEASUREMENTS BEHIND REFLECTED SHOCK WAVES IN AIR

For the period 1 April 1971 - 31 July 1972

Submitted by Jon B. Bader, Robert M. Nerem, Jonathan B. Dann, and Micheal A. Culp
Department of Aeronautical and Astronautical Engineering

Date 7 September 1972

ABSTRACT

A radiometric method for the measurement of gas temperature in self-absorbing gases has been applied in the study of shock-tube generated flows. This method involves making two absolute intensity measurements at identical wavelengths, but for two different path-lengths in the same gas sample. Experimental results are presented for reflected shock waves in air at conditions corresponding to incident shock velocities from 7 to 10 km/s and an initial driven tube pressure of 1 torr. These results indicate that, with this technique, temperature measurements with an accuracy of ±5 percent can be carried out. The results also suggest certain facility related problems.

TABLE OF CONTENTS

LIST OF FIGURES

LIST OF FIGURES - (Continued)

LIST OF TABLES

I. INTRODUCTION

During the past ten years, shock tubes have been used extensively in the experimental study of radiative transfer in shock-heated gases as well as in the study of other aspects of high temperature shock layer phenomena. The chief advantage in using a shock tube for such studies is the ability to produce high temperature gases at known conditions, i.e., at conditions which can be readily calculated for equilibrium states using the appropriate normal shock equations. Because of the relative ease with which such calculations are carried out, shock-tube studies in most cases have been limited to heat transfer measurements and to photometric measurements of either spectral or total radiative intensities, in addition to the normal measurements of incident shock-wave velocity and initial driven-tube pressure. The latter are of course necessary to calculate the equilibrium state of the shock-heated gas.

Temperature measurements have only been carried out in a very limited number of studies and their general importance has been somewhat minimized. This is understandable for many conditions of interest in shock-tube research and since such measurements are not easy. However, at low densities where nonequilibrium conditions may prevail and at high temperatures where radiative cooling may be important, the measurement of temperature becomes extremely important. Furthermore, recent measurements by Wilson and Wood[1,2] at the Lockheed Palo Alto Research Laboratory and by Bengston et al. at the University of Maryland,[3] call into question our ability to even calculate equilibrium conditions in shock-heated gases. The measurements of both of these investigations were carried out behind reflected shock waves and show discrepancies of approximately five percent between the data and equilibrium state calculations. It is this importance of temperature measurements in the understanding of nonequilibrium and radiatively cooled flows and the questions raised by the Lockheed and University of Maryland experiments which have motivated the experimental effort discussed herein.

The technical effort on this project, as originally proposed, in essence involved the use of various methods in the measurement of gas temperature behind both incident and reflected shock waves in air and other gases of interest in the study of planetary entry. The aim of these measurements was to be as follows: (i) to provide a comparative evaluation of different gas temperature measurement methods; (ii) to investigate the effect of radiative cooling behind reflected shock waves; and (iii) to investigate nonequilibrium effects, particularly, coupled radiation and nonequilibrium effects behind both incident and reflected shock waves. Originally there were to have been two phases to this study; the first phase was to have primarily involved the application of temperature measurement techniques already in use in shock tube studies at Ohio State. The second phase was to involve the application of other temperature measurement techniques to be determined on the basis of a literature review and assessment to be carried out

during the first phase. In addition to the general increase in the understanding of high temperature, radiating flows that would have resulted from this research, part of the motivation for this effort was that the experience gained with the techniques used would be of direct benefit to the work going on in the Hot Gas Radiation Research Facility at the NASA Langley Research Center and in the development of a temperature measurement technique for this facility.

Unfortunately, it was apparent early in the project that there would not be a second phase to this effort. The focus of the program was thus somewhat changed to center on the development of a technique that would lend itself to a day-to-day, on-line use with the NASA Langley Hot Gas Radiation Research Facility. Because of the questions which have arisen regarding the validity of equilibrium gas temperature calculations and the effects of nonequilibrium and radiative transfer phenomena, it was felt that the development of such a capability would enhance their research effort.

The following section will review some of the types of methods widely used to measure gas temperatures which were investigated in the early portion of this study. Following this, for reasons to be discussed later, it was decided that the focus of this effort would be on radiometric, as opposed to spectroscopic, measurement techniques. The ensuing measurements were carried out behind reflected shock waves in air at an initial driven-tube pressure of 1 torr and for incident shock velocities ranging from 7 to 10 km/s. These shock tube conditions were chosen because it appeared that the resulting post-reflected shock wave conditions would correspond approximately to the post-incident shock wave conditions associated with on-going NASA Langley studies. Air was used as a test gas because of the extensive information available on its thermodynamic and radiative properties; however, the Double Absolute Intensity Measurement (DAIM) technique finally used is felt to have application to a wide range of gases. In fact, one of its advantages is that its use does not depend on knowledge of any gas properties.

As will be seen, the results obtained, though raising certain questions, have been encouraging. In addition to the general application of this technique to shock-tube produced flows, measurements have also been carried out under conditions where the effects of radiative cooling have been observed to occur. For these conditions, the results obtained have shown reasonable agreement with gas temperature predictions which include radiative transfer effects.

II. METHODS FOR THE MEASUREMENT OF GAS TEMPERATURE

The methods selected to be discussed in this section have been chosen on the basis of their applicability to the temperature range of approximately 10 to 20,000 K and a necessary response time of the order

of 1 μs. In all of these methods, the assumption of local thermodynamic equilibrium is made and, normally, a uniform slab (possibly with time varying properties) of test gas is assumed. These temperature methods are broken down into two broad classes of methods: (1) methods applicable to transparent or optically thin gases, and (2) methods applicable to self-absorbing gases. Additional information on these and other methods may be found in References 4 and 5.

Transparent gas methods assume that the optical depth is small (i.e., $\tau_\lambda \ll 1$) or, in other words, that self-absorption is negligible in the wavelength region of interest. The simplest of the transparent gas techniques is the relative line intensity ratio method, sometimes called the two-line technique. This method has been used here at Ohio State to measure temperatures in shock-heated xenon.[6] The method is based on the fact that the integrated intensity of a line due to a transition from some upper energy level E_U to some lower energy level E_L can be written as

$$I_{UL} = N_U A_{UL} \frac{hc}{\lambda} \frac{\ell}{4\pi} . \tag{1}$$

Here I_{UL} is the integrated intensity of the line, N_U is the number density of particles in the upper energy level, A_{UL} is the Einstein coefficient for spontaneous emission or the transition probability, λ is the wavelength associated with the transition from the upper to the lower energy state, ℓ is the path length of the radiating slab, and h and c are the Boltzmann constant and the speed of light, respectively.

The ratio of the intensity of two such atomic line transitions (subscripted 1 and 2 below) may be written for an optically thin gas as

$$\frac{I_1}{I_2} = \frac{N_1}{N_2} \frac{A_1}{A_2} \frac{\lambda_2}{\lambda_1} \tag{2}$$

Furthermore, for local thermodynamic equilibrium, the number density ratio N_1/N_2 can be expressed as a function of the temperature T from the Boltzmann distribution as

$$\frac{N_1}{N_2} = \frac{g_1}{g_2} \exp\left[(E_2 - E_1)/kT\right] \tag{3}$$

where g_1 and g_2 are the statistical weights or degeneracies of the upper states, having energies E_1 and E_2, involved in the two measured transitions. Substituting and rearranging yields the gas temperature as a function of the intensity ratio and the atomic properties

$$T = \frac{E_2 - E_1}{k \ln\left(\frac{I_1}{I_2} \frac{\lambda_1}{\lambda_2} \frac{g_2 A_2}{g_1 A_1}\right)} \qquad (4)$$

In some cases, line ratio techniques can be extended to lines which originate from different states of ionization by further assuming, as an example, Saha equilibrium. Saha expressions can then be used to relate the number densities of different species. This, however, must be applied with great care.

Using a similar approach to that used in the line intensity ratio techniques, some work has been done using the ratio of continuum intensities at two wavelengths. Line to continuum intensity ratio methods have also been used. These methods, however, are not in wide use due to the lack of detailed knowledge of the collision cross-sections and Gaunt factors necessary in continuum intensity predictions.

A method of considerable use in temperature measurements, however, is the absolute line intensity technique. Absolute line intensity measurements by themselves actually yield only the number density N_U of the upper energy level of the transition. If in addition to the intensity measurement an absolute pressure measurement is made, then from equilibrium considerations the temperature can be calculated. A slightly different, but more involved, method requires not only an absolute integrated intensity measurement for the line, but also a measurement of the line profile. From these two measurements the temperature then can be inferred through an iteration technique. In Reference 3 measurements of this general type are reported for shock-heated neon where small percentages of spectroscopic additives were present. Both the 5852 Å line of neon and the H_α line were used. Similar measurements are reported for air in References 1 and 2 using several different nitrogen and oxygen line transitions.

Another method for determining temperature based on an absolute intensity measurement uses the absolute intensity of a continuum region. Although the theoretical prediction of continuum absolute intensities is difficult because of the necessary knowledge of radiative cross-sections, temperature measurements using selected continuum regions in N and O have been compared with the results of other temperature methods and seem to indicate that continuum intensity measurements of temperature are feasible.[1,2,7] This method also has the added advantage of high temperature sensitivity relative to other techniques. Again this type of measurement requires an additional measurement and may involve the assumption of equilibrium and/or an iteration technique in order to reduce the intensity measurement into a temperature measurement.

Finally, the broadening of atomic lines may also be used to determine the temperature of a gas. This involves the measurement of the relative intensity of the line profile and then a comparison of this

measured profile (or half-width) with tabulated or calculated profiles. Line broadening techniques can only be applied to lines (gases) that are fairly well understood and in which the broadening mechanisms are known. For example, the hydrogen H_α and H_β lines are good choices, and the use of these in measurements behind reflected shock waves in air are reported in References 1 and 2. To apply broadening techniques in other gases, normally the test gas is seeded with a small amount of hydrogen in order to use its well-known properties. The measurement of hydrogen line broadening (Stark broadening) gives a direct measurement of the electron density and not the gas temperature. The temperature must be inferred from the electron density measurement and an additional measurement. It should be recognized that the use of a seeding material always raises questions about the validity of the results obtained. This is particularly true in nonequilibrium situations where the added material may act as a contaminant and alter the normal relaxation processes.

In contrast to the above methods, which are based on the assumption of a transparent gas, are the methods applicable to a gas of finite optical thickness, i.e., a self-absorbing gas. The effect of absorption on the intensity from an optically thick spectral region of a uniform gas may be simply expressed as

$$I_\lambda = B_\lambda[1 - \exp(-\tau_\lambda)] \tag{5}$$

where I_λ is the observed intensity from the gas at a wavelength λ, B_λ is the blackbody intensity at the wavelength λ for a temperature T, and τ_λ is the optical depth.

The blackbody or brightness temperature method is applicable if the optical depth is much greater than order one ($\tau_\lambda \gg 1$). Then, from the above equation, the observed intensity I_λ approaches the blackbody intensity, $I_\lambda \simeq B_\lambda$, where B_λ is given as

$$B_\lambda = \frac{C_1}{\lambda^5} \frac{1}{\exp(C_2/\lambda T) - 1} \tag{6}$$

B_λ, for a given wavelength λ, is only a function of temperature. Thus, a measurement of the gas temperature T can be made by an absolute intensity measurement of the emitted radiation I_λ at some wavelength λ and by equating this intensity to that of a blackbody. Although certainly not the first to carry out such measurements, Bader[8] at Ohio State applied this technique to shock-heated xenon using the 5292 Å Xe^+ transition. Measurements of this type have also been reported in the literature for air;[2] however, in this case the gas was seeded with hydrogen and the H_α line was used. It should be noted that an optical thickness τ_λ greater than order one will frequently occur

only at the center of the more intense lines. Thus, in using this method to measure temperature, care must be taken to ensure that the gas is optically thick at the wavelength selected. One must also ensure that the measured intensity is not adversely affected by radial gradients, e.g., by absorption in the boundary layer region near a wall.

When the gas is not optically thick enough for the brightness temperature method to be used, but too optically thick to neglect absorption processes, then the two line intensity ratio technique may be used with suitable corrections. This is, in fact, how this technique was used in the temperature measurements reported in Reference 6. The details of this correction procedure are reported in Reference 9. The other optically thin temperature measurement methods may be similarly corrected for absorption effects; however, in almost all cases, this becomes extremely tedious.

Another method which relies on absorption for its use is the so-called line reversal method. In the application of this technique, one endeavors to determine the intensity level of a known source at which the gas radiation is indistinguishable from the background source radiation, i.e., it appears neither in emission or absorption. This technique has been applied to a variety of gases with somewhat mixed results. Normally a seed gas is used, e.g., either sodium or hydrogen;[3] however, in the limit of the gas becoming optically thick, then the gas radiation itself can be used with no seeding being necessary.

A modification of the line reversal method is the so-called emission-absorption method. As in the previously discussed brightness temperature method, the radiated intensity I_λ is measured. In addition to this measurement, a measurement of a lamp of known intensity I_{λ_L}, as viewed through the test gas, is made. The known intensity of the lamp I_{λ_L} will be attenuated as it passes through the test gas by the factor $\exp(-\tau_\lambda)$. Thus, this second intensity measurement is the sum of the gas radiation plus the attenuated lamp radiation, or

$$I_{\lambda_T} = I_\lambda + I_{\lambda_L}\exp(-\tau_\lambda) \tag{7}$$

where I_{λ_T} is the total measured intensity. This expression can be combined with Eq. (5) to yield the blackbody intensity B_λ or, effectively, the gas temperature as a function of the two measured intensities I_λ and I_{λ_T}, and the known lamp intensity I_{λ_L}. Thus, by measuring the two intensity ratios I_λ/I_{λ_L} and $I_{\lambda_T}/I_{\lambda_L}$, and knowming the absolute intensity of the lamp I_{λ_L}, the gas temperature can be computed. This general emission-absorption approach to temperature measurement can be applied to either line or continuum radiation provided the optical thickness is not too small and that the lamp intensity is approximately equal to the gas intensity. The necessary optical thickness is normally only achievable using hydrogen as a seed gas.[3]

Still a further evolution of this method is what will be referred to here as the Double Absolute Intensity Measurement (DAIM) technique. In this method the absolute intensity of the gas is measured over two different path lengths. These two measured intensities, I_{λ_1} and I_{λ_2}, are related to the gas properties through the relations

$$I_{\lambda_1} = B_\lambda[1 - \exp(-\tau_{\lambda_1})]$$
$$I_{\lambda_2} = B_\lambda[1 - \exp(-\tau_{\lambda_2})] \tag{8}$$

where $\tau_{\lambda_1} = \tau_{\lambda_2}(\ell_1/\ell_2)$ and ℓ_1, ℓ_2 are the two path lengths. If I_{λ_1} and I_{λ_2} are measured and with ℓ_1 and ℓ_2 known, then the above equations are sufficient to calculate the blackbody function, B_λ, and thus, the temperature. In addition, the optical thickness can be determined. This is equally true of the emission-absorption method, and in fact, the only difference between that method and DAIM is that in the latter an external source is not required.

It is of interest to note that the brightness, line reversal, emission-absorption, and DAIM techniques all do not require any atomic information about the gas being tested (e.g., transition probabilities, broadening parameters, number densities, collision cross-sections, etc). Thus, these methods eliminate errors due to incorrect values of parameters which are typically hard to measure. This and the resulting simplicity of the data reduction procedure are attractive from the viewpoint of making temperature measurements on a routine, day-by-day, on-line basis using a variety of test gases in which the use of seeding is either undesirable or impractical.

It was for these reasons that this class of methods was chosen for application in the present program. Initial efforts were directed towards the application of the brightness temperature method using the 6490 Å multiplet of nitrogen, and preliminary brightness temperature measurements were carried out. Questions raised by the possibility of insufficient gas optical thickness for the use of this method resulted in the decision to develop DAIM, in which two absolute intensity measurements at the same wavelength, but different path lengths, are used as previously described to determine the gas temperature and optical thickness. In this application the 6490 Å nitrogen transition was again used.

This method is most suitable when the gas is neither too optically thin nor too optically thick. In the latter case, of course, this method reverts to the brightness temperature method since $I_{\lambda_1} = I_{\lambda_2} = B_\lambda$; and in the former case the accuracy becomes very poor. This will be discussed further in the next section.

One of the advantages of DAIM is that it not only yields temperature, but also optical thickness, such that one can then assess whether or not the gas is sufficiently optically thick for the use of the method itself. If it is not, then one can turn to using one of the optically thin methods, e.g., the two-line relative intensity method or the absolute line intensity method.

There are of course other methods for the measurement of gas temperature not discussed here. Various hydrodynamic methods have been used which are based on determining the speed of sound of the gas, e.g., through a measurement of the Mach angle. Such measurements, though interesting, are impractical for use on a routine basis as should be obvious. There are also methods based on X-ray spectroscopy; however, these methods are largely limited to temperatures corresponding to energies above 100 eV. Finally, lasers also have been used as a diagnostic tool to investigate gas properties, including temperature. In the latter, the laser is used as a high intensity light source in a scattering-type experiment. The laser beam is passed through the gas, and the spectrum of the scattered radiation is measured at different scattering angles. One of the possible advantages of laser scattering methods over present techniques is the possibility of measuring not only electron temperatures, but also measuring heavy body temperatures directly. However, such laser diagnostic technqiues are still in their infancy and need to be further explored.

Thus, of all the techniques discussed here, it is the Double Absolute Intensity Measurement method - DAIM - which appears to be the most attractive within the constraints of the present program. As was indicated earlier, an initial effort to carry out brightness temperature measurements led to the development of DAIM. In the following sections, theory underlying both brightness temperature and the DAIM techniques will be considered further. In addition, the experimental arrangement used in the measurements reported herein will be discussed.

III. BASIC CONCEPTS OF BRIGHTNESS AND DAIM TECHNIQUES

The brightness and Double Absolute Intensity Measurement (DAIM) techniques will be discussed in terms of the inherent assumptions, the expected sensitivity, and the potential advantages and disadvantages of each technique.

Both the brightness and DAIM techniques have a number of basic assumptions in common. The first of these is that the gas of interest is assumed to be in local thermal equilibrium in the sense that all translational, rotational, vibrational, and electronic modes can be ascribed the same temperature T. However, the gas is not necessarily assumed in chemical (Saha) equilibrium. Second, the gas under observation is considered to possess uniform properties at any instant of time

but that these properties may vary with time. Finally, the gas is assumed to be absorbing and emitting (including induced emission), but scattering is negligible for the test gas sizes of interest.

In addition, the unsteady term in the equation of radiative transfer is assumed negligible. The solution to the equation of radiative transfer applicable under these assumptions for a slab of gas of thickness ℓ then takes the form

$$I_\lambda = B_\lambda[1 - \exp(-k'_\lambda \ell)] \tag{9}$$

where I_λ is the emergent radiative intensity at wavelength λ (in W/cm^2-sr-μm), k'_λ is the linear absorption coefficient (in cm^{-1}) at wavelength λ including induced emission, and B_λ is the Planck blackbody intensity at wavelength λ(in W/cm^2-sr-μm). The Planck blackbody intensity can be expressed as

$$B_\lambda = \frac{C_1/\lambda^5}{\exp(C_2/\lambda T) - 1} \tag{10}$$

where C_1 is the first radiation constant equal to $2hc^2$ (11,910 W-μm^4/sr-cm^2), C_2 is the second radiation constant equal to hc/k (14,390 μm-K), λ is the wavelength under observation (in μm), and T is the gas temperature (in Kelvin).

When the optical thickness $\tau_\lambda = k'_\lambda \ell$ is sufficiently large ($\tau_\lambda \simeq 5$), the exponential term in Eq. (9) will be very small compared to unity, and the observable intensity I_λ will be very nearly equal to the Planck blackbody intensity B_λ, i.e., $I_\lambda \simeq B_\lambda$. Since the Planck blackbody intensity at wavelength λ is only a function of temperature, the gas temperature T can be written as an explicit function of the observable intensity I_λ and the wavelength of observation λ in the form

$$T = \frac{C_2/\lambda}{\ell n[1 + C_1/(I_\lambda \lambda^5)]} \tag{11}$$

This measurement approach is denoted as the brightness or blackbody technique. The only additional assumption necessary over the basic assumptions mentioned earlier is that the gas possess sufficient opacity at the wavelength of observation, i.e., $\tau \simeq 5$. If this condition is not met, the measured intensity will be less than the blackbody intensity, and the calculated temperature will be less than the actual gas temperature.

The Planck blackbody temperature-intensity relationship of Eq. (10) is shown graphically in Fig. 1 for various wavelengths. An idea of the sensitivity (percent change in intensity corresponding to a percent change in temperature) of a brightness type of measurement can be obtained by differentiating the Planck expression, Eq. (10), with respect to temperature, which yields, after some rearrangement,

$$\frac{dI_\lambda}{I_\lambda} = S \frac{dT}{T} \tag{12}$$

where

$$S = \frac{C_2}{\lambda T} \frac{\exp(C_2/\lambda T)}{[\exp(C_2/\lambda T) - 1]} \tag{13}$$

The parameter S is representative of the experimental accuracy that can be expected from a brightness temperature measurement. For example, if the parameter S (sensitivity parameter) is 2, a 10 percent error in the intensity measurement corresponds approximately to a 5 percent error in the corresponding temperature. This sensitivity parameter S is presented as a function of temperature for various wavelengths in Fig. 2. It can be seen from this figure that as the temperature increases, S decreases (for a given wavelength) asymptotically approaching 1. Conversely, as wavelength decreases, S increases (for a given temperature). Thus it is desirable, from the viewpoint of experimental accuracy, to operate at short wavelengths. The choice of the wavelength region, however, is normally dictated by the spectral features available in the particular gas under investigation. For the temperature range of 10,000 to 20,000 K, a sensitivity factor of 1.5 to 4 can be expected in the visible wavelength region. In the vacuum-ultraviolet region of 1000 to 2000 Å and for the same temperature range, the sensitivity is of the order of 4 to 15. However, additional experimental difficulties are encountered making measurements in the vacuum-ultraviolet region which may offset this advantage. In the near infrared region ($0.7 < \lambda < 10$ μm) the sensitivity S will be near unity, making the temperature measurement only as accurate as the absolute intensity measurement. However, the large disparity between calibration intensities and plasma intensities encountered in the visible and ultraviolet wavelength regions is reduced in the infrared by an order of magnitude or more. This possibly off-sets any disadvantage due to low sensitivity for this region.

The normal justification for the application of a brightness technique is based on a preliminary estimate of the opacity τ of a spectral feature of the radiation field (e.g., an atomic line, or intense continuum region, or combination of a number of radiative processes) and

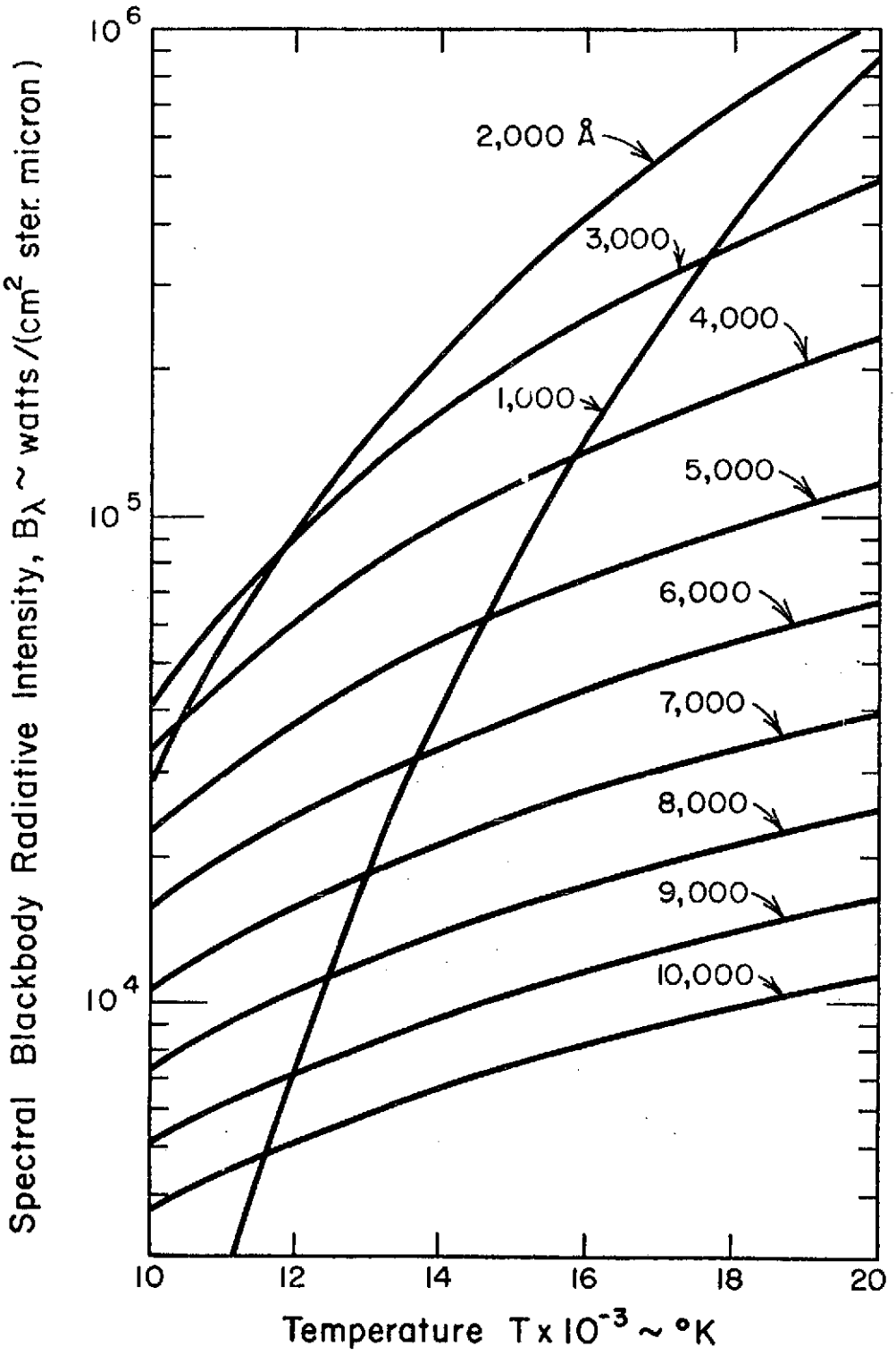

Fig. 1. Spectral Blackbody Radiative Intensity as a Function of Temperature

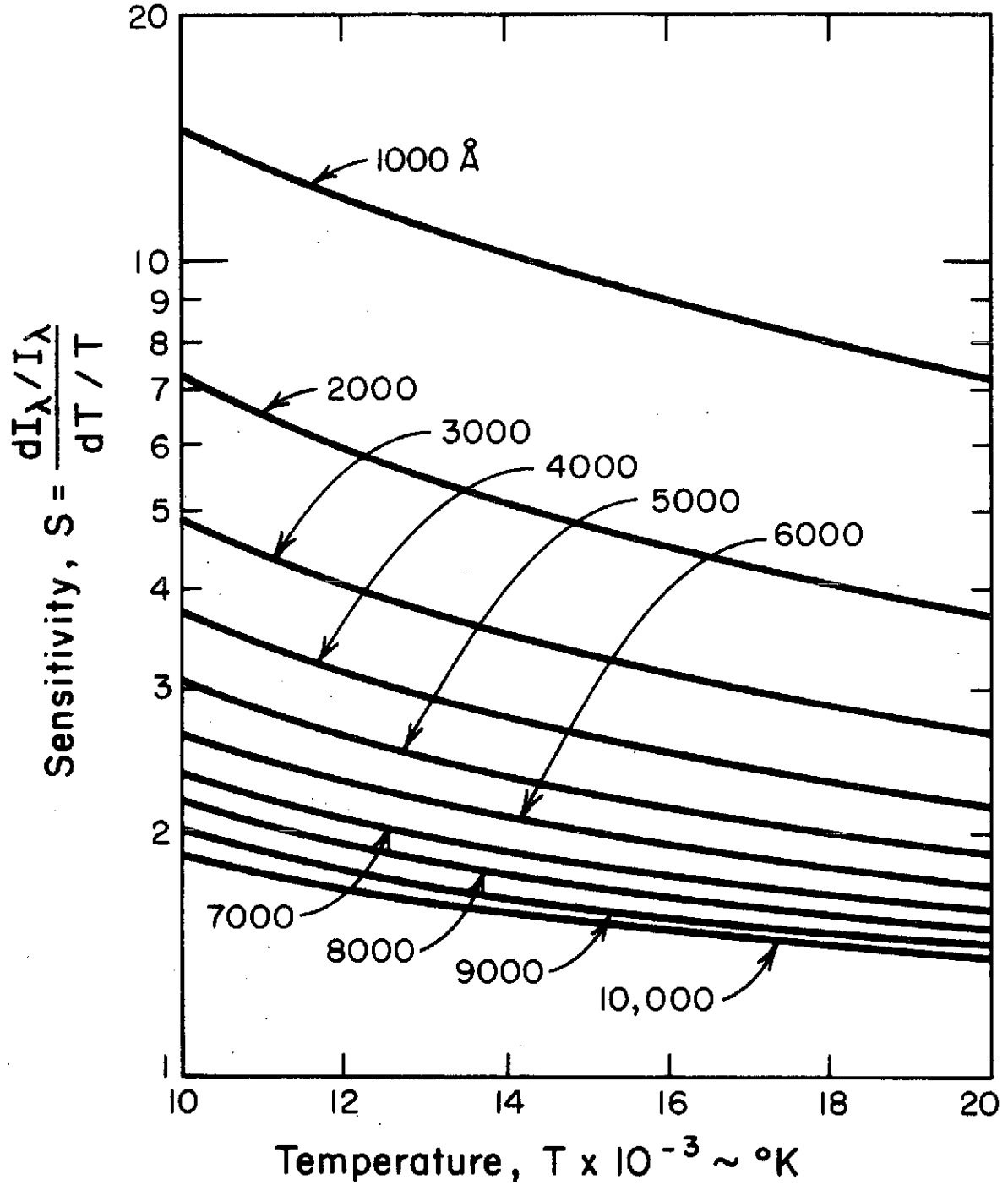

Fig. 2. Sensitivity Parameter for Brightness Temperature Measurement

its wavelength extent. If the required opacity is not available to justify a brightness measurement but is still large, (e.g., $\tau \sim 1$ or greater), then the Double Absolute Intensity Measurement (DAIM) technique may be applied.

The basic concept behind the DAIM technique is to obtain measurements of the absolute intensity of the radiation at a wavelength λ emerging from a uniform slab of gas for two physically different path lengths ℓ_1 and ℓ_2. The equations describing the emerging radiative intensity for these two paths are

$$I_{\lambda_1} = B_\lambda[1 - \exp(-k'_\lambda \ell_1)] \tag{14}$$

$$I_{\lambda_2} = B_\lambda[1 - \exp(-k'_\lambda \ell_2)] \tag{15}$$

where the subscripts 1 and 2 denote the two different paths.

By measuring the absolute intensities I_{λ_1} and I_{λ_2}, the wavelength of the radiation λ, and the path lengths ℓ_1 and ℓ_2, the gas temperature T can be calculated from the above two equations and the Planck expression, Eq. (10). In addition to the gas temperature T, the absorption coefficient k'_λ of the gas can also be determined. The above two equations cannot be solved explicitly for T or k'_λ, thus making the temperature-intensity and opacity-intensity relationships less clear. However, by dividing Eq. (15) by Eq. (14) the optical thickness of path 1 (τ_1) can be written as an implicit function of only the ℓ_2/ℓ_1 and $I_{\lambda_2}/I_{\lambda_1}$ ratios in the form

$$\frac{I_{\lambda_2}}{I_{\lambda_1}} = \frac{1 - \exp(\tau_1)}{1 - \exp\left(\tau_1 \frac{\ell_2}{\ell_1}\right)} \tag{16}$$

where $\tau_1 = k'_\lambda \ell_1$. This opacity-intensity ratio relationship is shown in Fig. 3 for various ℓ_2/ℓ_1 ratios.

To illustrate the DAIM concept further, a plot of I_{λ_2} versus I_{λ_1} with constant temperature and constant τ_1 lines is shown in Fig. 4 for a wavelength of $\lambda = 6490$ Å and a path length ratio $\ell_2/\ell_1 = 1/4$ (these are the values used in the present experimental measurements). Note that when the optical thickness τ_1 is infinite, $I_{\lambda_1} = I_{\lambda_2} = B_\lambda$ and the DAIM technique reverts into two brightness temperature measurements. As the opacity of the gas decreases (for a given temperature to $\tau_1 \simeq 5$, the observable intensity I_{λ_1} is not appreciably different from the Planck blackbody function B_λ (approximately 0.3% less). However, as τ_1 decreases from infinity to $\tau_1 = 5$, τ_2 decreases from infinity

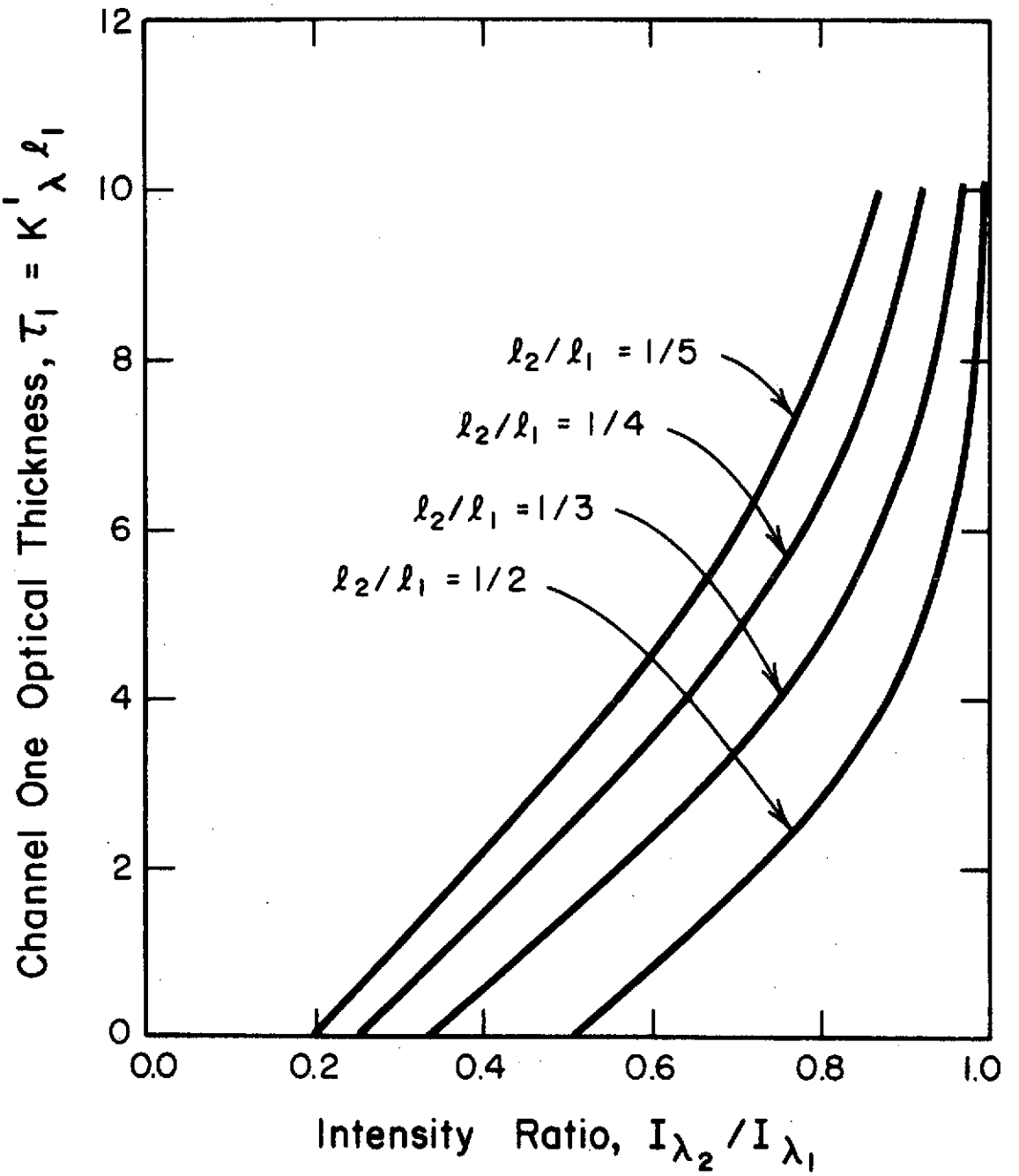

Fig. 3. Optical Thickness for Path Length of Channel 1 of DAIM System as a Function of Intensity Ratio

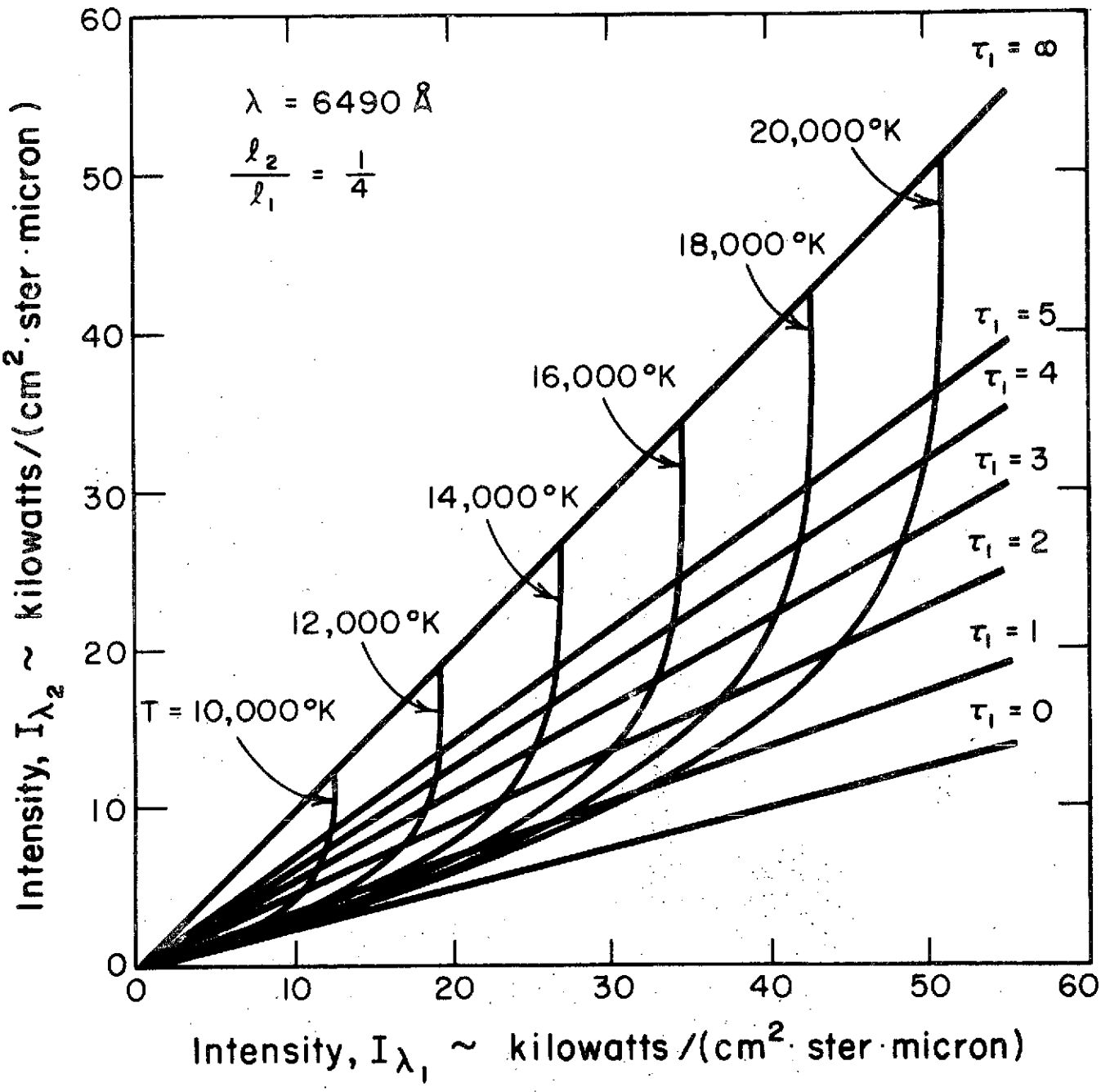

Fig. 4. Representation of Measured Temperature as a Function of Measured Intensities from Channels 1 and 2 of DAIM System for Path Length Ratio $\ell_2/\ell_1 = 1/4$ and $\lambda = 6490$ Å

to 1.25 and thus I_{λ_2} is appreciably less than B_λ (approximately 30% less). Furthermore, as the optical thickness approaches zero, the gas becomes transparent, and the observable intensity ratio $I_{\lambda_2}/I_{\lambda_1}$ approaches the path length ratio ℓ_2/ℓ_1, becoming independent of the gas temperature T. Thus, at small optical thickness, the DAIM measurement technique will become experimentally inaccurate.

In order to obtain a more quantitative idea of the range of optical thickness τ that will yield reasonable experimental accuracy (sensitivity) in a temperature measurement, a sensitivity parameter $S_{I_\lambda} = dI\lambda/I\lambda/dT/T$ can be obtained for either intensity I_{λ_1} or I_{λ_2} by differentiating Eq. (14) with respect to temperature holding I_{λ_2} constant, or differentiating Eq. (15) with respect to temperature holding I_{λ_1} constant. This yields, after some rearrangement

$$\left.\frac{dI_{\lambda_1}/I_{\lambda_1}}{dT/T}\right|_{I_{\lambda_2} = \text{const.}} \equiv S_{I_{\lambda_1}} = S\left\{1 - \frac{\ell_1}{\ell_2}\,\frac{\left[\exp\left(\tau_1\,\frac{\ell_2}{\ell_1}\right) - 1\right]}{\left[\exp(\tau_1) - 1\right]}\right\} \tag{17}$$

$$\left.\frac{dI_{\lambda_2}/I_{\lambda_2}}{dT/T}\right|_{I_{\lambda_2} = \text{const.}} \equiv S_{I_{\lambda_2}} = S\left\{1 - \frac{\ell_2}{\ell_1}\,\frac{\left[\exp(\tau_1) - 1\right]}{\left[\exp\left(\tau_1\,\frac{\ell_2}{\ell_1}\right) - 1\right]}\right\} \tag{18}$$

where S is the same sensitivity parameter as that for the brightness technique given in Eq. (13) and displayed in Fig. 2

$$S = \frac{C_2}{\lambda T}\,\frac{\exp(C_2/\lambda t)}{\left[\exp(C_2/\lambda T) - 1\right]} \tag{19}$$

The sensitivity parameters $S_{I_{\lambda_1}}$ and $S_{I_{\lambda_2}}$ normalized by the brightness sensitivity S are shown in Figs. 5 and 6 as a function of optical thickness τ_1 for various path length ratios ℓ_2/ℓ_1.

It can be seen from these two figures that the sensitivities $S_{I_{\lambda_1}}$ and $S_{I_{\lambda_2}}$ can be improved by using a small ℓ_2/ℓ_1 ratio. However, the smallest ratio experimentally practical will be determined primarily by the physical size of the facility available and the wall thermal boundary layers (which at present are being neglected). Thus, the ℓ_2/ℓ_1 ratio should be optimized for a given facility and physical problem under investigation.

The sensitivity parameter $S_{I_{\lambda_1}}$ will always be less than the sensitivity parameter S of the brightness technique at the same wavelength λ. The sensitivity parameter $S_{I_{\lambda_2}}$ is much larger than S for

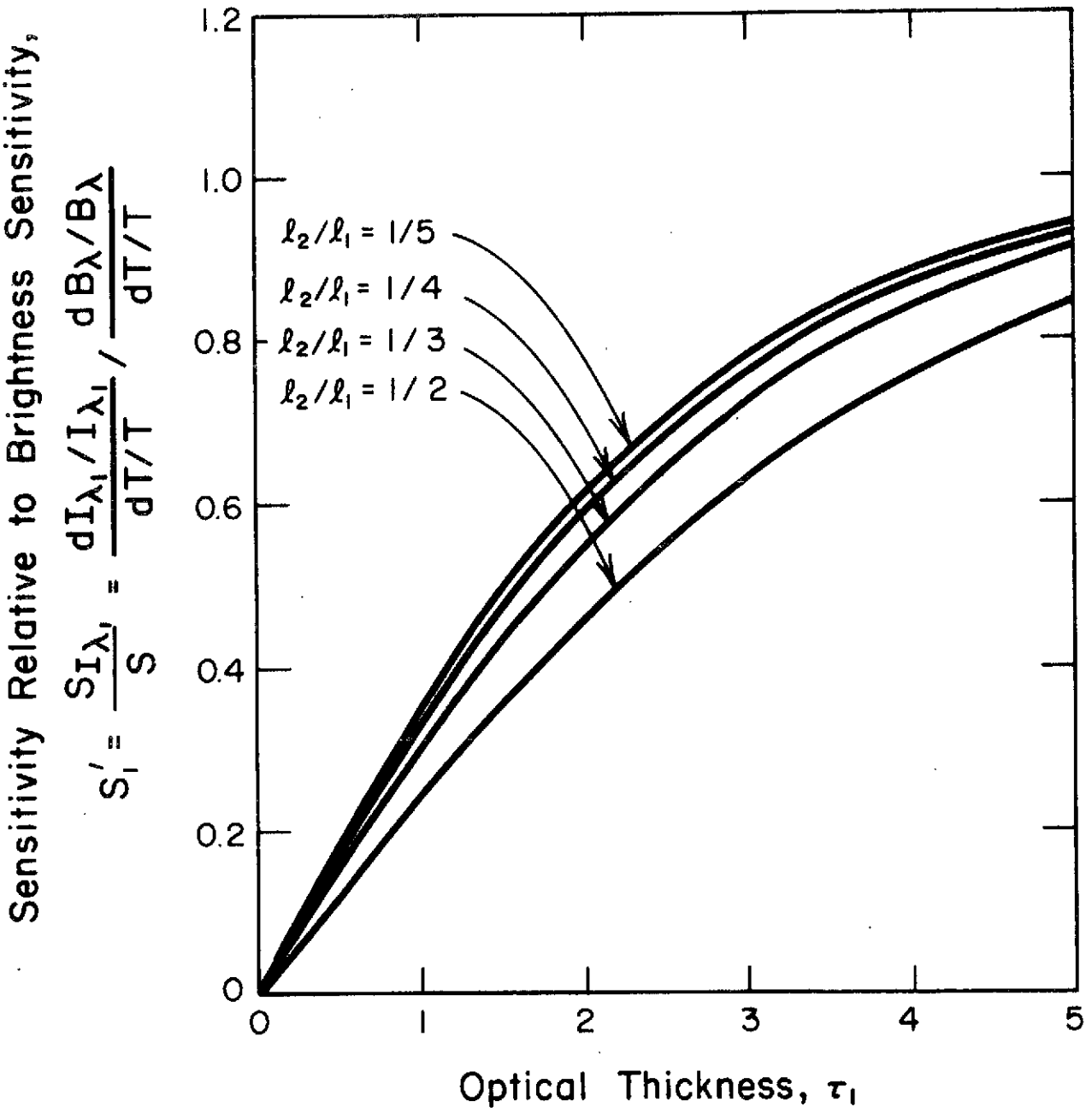

Fig. 5. Relative Sensitivity Parameter for Channel 1 of DAIM System

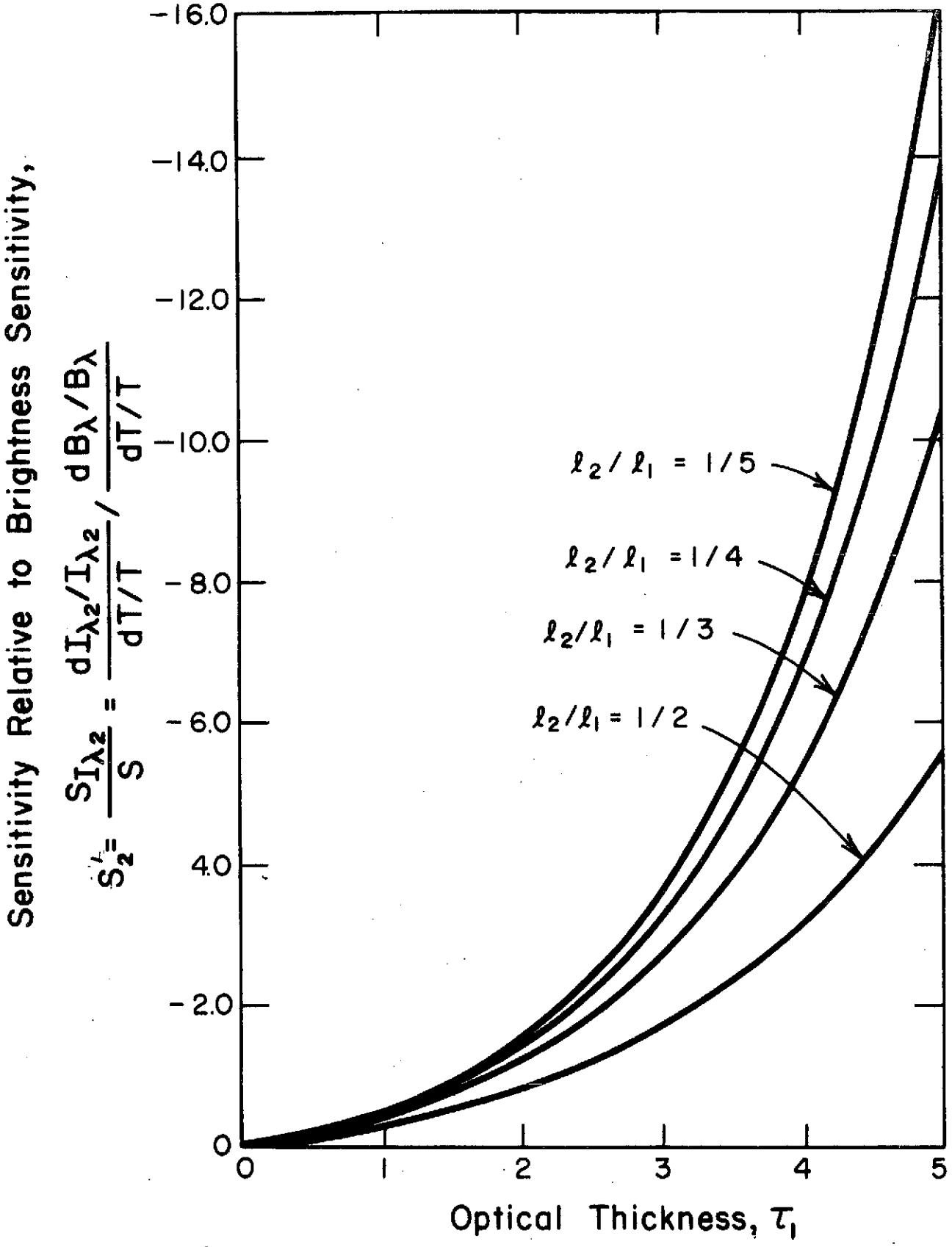

Fig. 6. Relative Sensitivity Parameter for Channel 2 of DAIM System

large τ_1, but eventually drops to less than S for small τ_1 values. The experimental accuracy of the DAIM technique will be primarily determined by $S_{I_{\lambda_1}}$, especially at large τ_1, and is inherently less sensitive (accurate) than that of the brightness technique (for the same wavelength λ). The overall accuracy that can be obtained from a DAIM temperature measurement is determined by the accuracy of the absolute intensity measurements that must be made, the wavelength of observation, and the opacity of the gas under observation. With considerable experimental care, absolute intensity measurements in the 3 to 5 percent range should be within the limits of the present state of the art. For example, measurements at a wavelength of 6000 Å would yield temperature measurements with accuracies of 1.5 to 2.5 percent for large τ_1 values ($\tau_1 \simeq 5$ or greater). This accuracy would be degraded by a factor of two (to 3-5 percent) for an optical thickness τ_1 of the order of 1.5 to 2 (depending on the ℓ_2/ℓ_1 ratio selected). Experimentally, there will be a lower limit on τ_1 which will yield acceptable experimental accuracy depending on (1) the accuracy requirements, (2) the wavelength under observation, and (3) the accuracy with which the absolute intensity measurements can be made.

Before discussing the actual applications of the brightness and DAIM techniques, it is worth mentioning that the above discussion was for a given wavelength λ. In practice, a wavelength region $\Delta\lambda$ will be under observation. If the absorption coefficient k'_λ is relatively constant over $\Delta\lambda$ and the wavelength extent $\Delta\lambda$ is not too large, then the above discussion is applicable to the center of this wavelength region. Even if there is considerable k'_λ variation over $\Delta\lambda$, so long as the lowest k'_λ is such that $k'_\lambda \ell$ is of the order of 5 or greater, the brightness technique will still yield correct results. However, the DAIM technique will be much more sensitive to large k'_λ variations over the bandpass $\Delta\lambda$. Therefore, its application to such a wavelength region requires additional information as to the spectral variation of k'_λ. However, this type of problem can be avoided by reducing the bandpass $\Delta\lambda$ sufficiently to satisfy the assumption of $k'_\lambda \simeq$ constant over the region $\Delta\lambda$.

The brightness and DAIM "radiometric" techniques have a definite advantage over "spectroscopic" temperature measurement techniques in that they do not require any detailed knowledge about the gas properties, such as transition probabilities, line broadening parameters, and/or collision cross sections. Thus, they are well suited for exploration of gases of unknown properties by eliminating the problems associated with background continuua or other spectral features in the wavelength region of observation. They can eliminate potentially the need for using seed gases (spectroscopic additives), which inherently change the problem under investigation.

The radiometric techniques have the disadvantage of not being as sensitive as some spectroscopic techniques and they require accurate absolute intensity measurement(s). They are also susceptible to boundary

layer problems. The brightness technique has the inherent assumption on the magnitude of τ which is eliminated in the DAIM technique. The DAIM technique, however, is still limited to large values of τ.

IV. EXPERIMENTAL APPARATUS

The majority of the experimental effort was directed towards the development and evaluation of the DAIM concept as a usable experimental temperature measurement technique. The physical test problem selected for study was time-resolved temperature measurements behind reflected shock waves in air. The wavelength region selected for the DAIM and the brightness measurements was the center-most portion of the strong nitrogen multiplet at $\lambda = 6490$ Å. Because of the relatively large half-width of the multiplet ($\simeq 50$ Å), the spectral band-pass half-width of 5 Å was considered acceptable to satisfy the DAIM assumption of a nearly constant absorption coefficient over the wavelength region under observation. Preliminary brightness measurements using a system similar to one channel of the DAIM system to be described here indicated that the assumption of $\tau > 5$ was not satisfied at the lower shock velocities of this problem, but that the optical thickness τ was increasing with increasing shock velocity.

It was anticipated that radiative cooling effects would be observable at the higher incident shock velocities. This effect, coupled with the relatively slow reflected shock velocities (1 to 2 km/s), dictated that the observation region be relatively narrow. In addition to these flow imposed constraints, physical constraints were imposed by the diameter of the window ports available (13 mm) and the finite size of the tungsten lamp filament that was necessary in calibration of the optics (approximately 15 mm high by 3 mm wide).

A photograph of the experimental arrangement for the DAIM measurements is presented in Fig. 7, and a schematic of the final optical system used in the present measurements is shown in Fig. 8. This system consists of two parallel absolute intensity channels approximately 6.5 mm apart (centerline to centerline). These two channels were formed by two Baird-Atomic spectrograph entrance slits 0.2 mm wide located 40 cm apart, the plane formed by their axis being normal to the shock-tube axis and in line with two 13 mm diameter sidewall observation ports on opposite sides of the shock tube. The two independent collimated channels were formed by replacing the fishtail slides of the spectrograph slits with slides having two 2.5 mm apertures spaced 6.5 mm apart. In order to eliminate crosstalk between channels, an additional slide with two 3.0 mm apertures (again 6.5 mm centerline to centerline) was located midway between the two Baird spectrograph slits. With this arrangement, it was impossible for radiation passing through the upper aperture of the first slit to pass through the lower aperture of the second slit (and vice-versa). The radiation passing through the lower set of

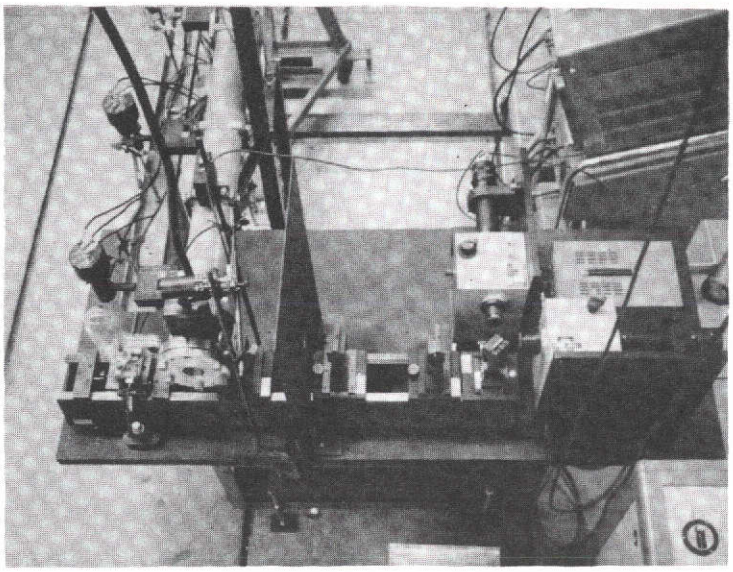

Fig. 7. Photograph of DAIM System

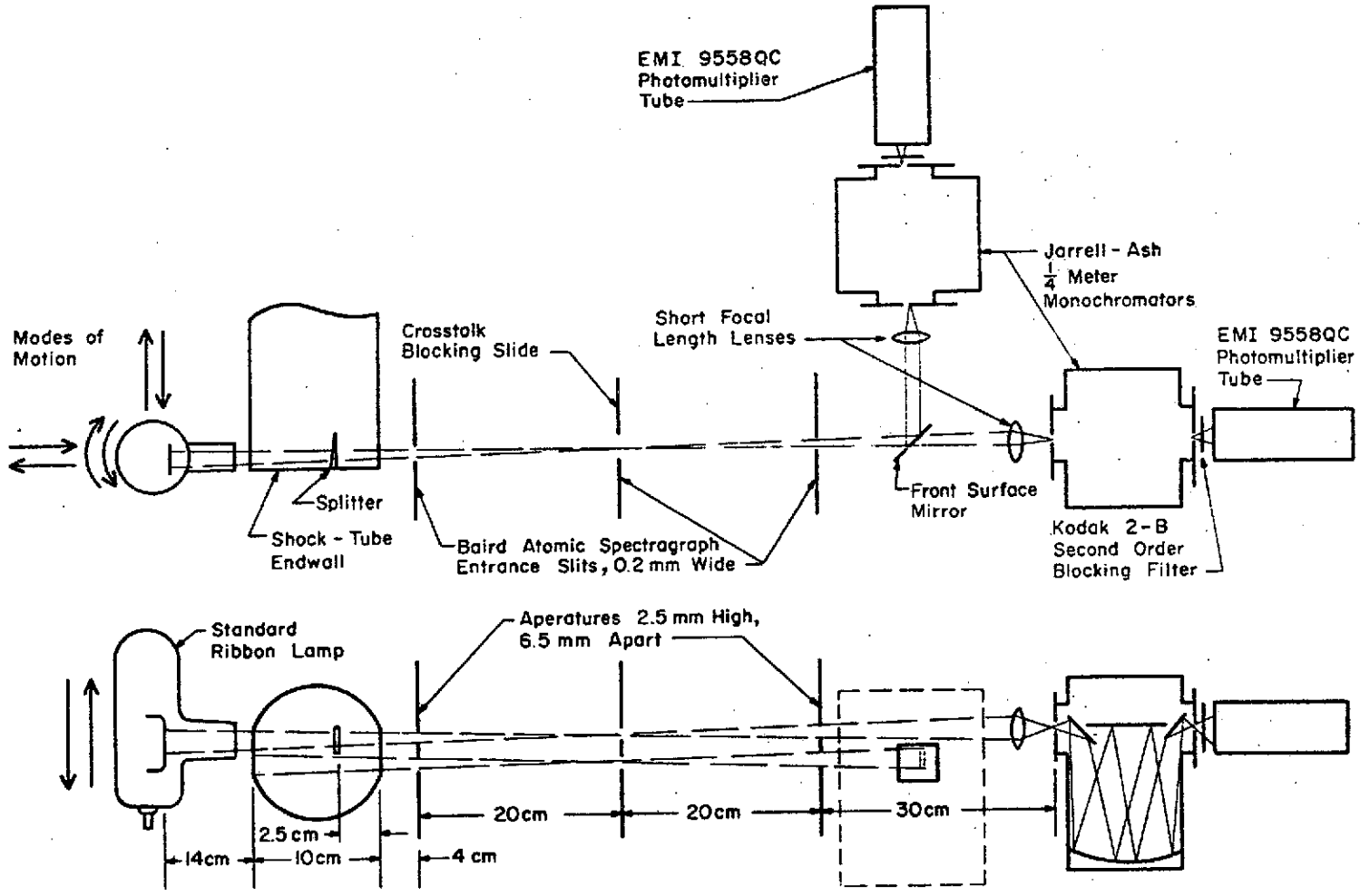

Fig. 8. Schematic of DAIM System

apertures was deflected at right angles using a front surface, aluminum deposited mirror.

The radiation passing through these collimated optical channels was then passed through f/3.5 Ebert mounted, Jarrell-Ash 1/4 meter grating monochromators to achieve the desired spectral resolution. These monochromators were equipped with fixed, straight, bayonet entrance and exit slits of 150 μm. These instruments have two interchangeable gratings, 2360 grooves/mm blazed at 3000 Å (16.5 Å/mm linear dispersion) and 1180 grooves/mm blazed at 5000 Å (33 Å/mm linear dispersion), the latter being used in the present measurements, yielding a bandpass half-width of 5 Å. In order to maintain good resolving power with the monochromators and reasonable collection efficiency, the collimating system and its respective monochromator were optically coupled together using a short focal length lens mounted directly on the monochromator entrance slit housing (1 1/4" focal length suprasil quartz lenses were used). This lens focused an extremely small image of the first slit aperture on the plane of the monochromator entrance slit (image height of the order of 0.1 mm). The monochromators were rotated 90°, making the entrance slits horizontal. This arrangement allowed the small image produced by each short focal length lens to be completely captured by the 0.15 mm entrance slit width. After passing through the entrance slit each beam diverged rapidly (due to the short focal length lens used), thus enabling good filling of the grating and, therefore, maintaining the instrument's resolving power. With this optical arrangement, very little of the slit height is actually used, and the unused portions of the entrance and exit slits were masked off to minimize stray light problems.

The radiation emerging from each exit slit was passed through a second-order blocking filter (a Kodak 2-B Wratten filter was used) and then converted into an electrical signal using an EMI 9558QC photomultiplier tube on each monochromator. These photomultiplier tubes were powered in parallel with a Keithley Model 244 High Voltage Power Supply, the voltage used varying run to run from 815 to 890 volts. (This voltage variation was used to eliminate scale changes in oscilloscope settings and, thus, recalibrations). Since the resultant peak currents expected in the photomultiplier tubes during a shock-tube run were in the 100 μA range, care was taken in the design of the dynode chain to keep the interstage voltage stable. This was accomplished by using a 150 V zener diode across the cathode to first dynode stage (as recommended by the manufacturer), 50 kΩ bleed resistors across all dynode stages, and 0.1 μF capacitors across the last four dynode stages.

The photomultiplier output currents during calibration were measured using two Keithley Model 414 Micro-Microammeters. During a shock-tube run, each photomultiplier output current was fed through 1.2 m of low capacitance coaxial cable (RF62B/U) to a 500 Ω load resistor (voltage drops across these resistors were 60 mV or less on each channel). The voltage developed across each load resistor was

displayed on a Tektronix 555 dual beam oscilloscope equipped with Type 1A7A plug-in units. The frequency response of the electronics was limited by the plug-in unit frequency discriminators to 1 MHz. The sensitivity of each radiation channel (which includes collimating slits, lens, monochromator, filter, and photomultiplier) was obtained by placing a tungsten ribbon lamp (General Electric Type T24-17 calibrated by Eppley Laboratories) on the opposite side of the shock tube from the collimating system. This arrangement caused the tungsten filament to completely fill the field of view of one channel of the collimating slit system. However, due to the large distance between the two collimated channels and the finite size of the ribbon filament, the lamp was installed on a vertical translator in order to alternately position the tungsten filament on the centerlines of the collimated channels while the lamp was in operation. In addition, horizontal translation in two directions and a rotation about the vertical axis were also incorporated in the system for proper positioning of the lamp. A calibration of each channel, using the standard ribbon lamp, was performed on each shock-tube run just prior to the actual test. To minimize time between calibration and the shock-tube test (evacuation and sample filling time), the calibration was performed through an additional window on the lamp side of the shock-tube while the shock-tube was at vacuum. The finite transmissivity of this window was taken into account in the data reduction. The windows used were 3 mm thick pyrex discs which were replaced after every shock-tube run.

The different physical path length needed for the second (upper) channel was obtained using a small flow divider extending from the endwall. This flow divider, or splitter, consisted of a half wedge 9 mm high, 8 mm wide, and with a half wedge angle (taper angle) of 7.5°. The surface of the splitter normal to the endwall was located 2.5 cm from the viewing window. With the splitter rotated into position, the field of view of the upper channel was terminated by the splitter surface while the lower channel extended the full width of the shock tube, unobstructed by the splitter. This arrangement gave the path length ratio selected for the present measurements, 4 to 1 (10 cm to 2.5 cm). In order to reduce reflections, the splitter was coated with flat black absorbing paint. In addition, carbon depositing on the splitter by the facility was allowed to build up over a number of runs. Based on initial estimates of the thermal boundary layer on the endwall (of the order of 1 mm), the region of observation was located 3.6 mm from the endwall. Side wall boundary layer effects for the expected test times of 10 μs were neglected.

From the spectral radiance (intensity) of the ribbon lamp at the desired wavelength and the measurements of the current ratios between the lamp and the shock-heated gas over the path lengths ℓ_1 and ℓ_2, the absolute intensity from the gas at the desired wavelength for the two path lengths was determined (again, linearity of the optical system, detector, and electronics is assumed). From measurements of I_{λ_1} and I_{λ_2} (and measurements of λ, ℓ_1, and ℓ_2) the DAIM temperature, T_m, was

obtained numerically from Eqs. (11), (14), and (15). The brightness temperature measurement is simply a blackbody intensity interpretation of channel 1 (lower physical channel) intensity. The brightness temperature T_{Br} can be calculated directly by using Eq. (11).

A selected oscillogram output from the 555 dual beam oscilloscope is shown in Fig. 9. The upper trace is for channel 1 (the 10-cm path length) and the lower trace is for channel 2 (the 2.5-cm path length). Also shown are zero lines, and directly below each trace is a time mark signal consisting of marks every μs (the zero lines and time marks were overlaid immediately before or after each shot). The time marks are from the same source and are used to ensure time syncronization of the two traces. Note the undesirable trace oscillations which are shot noise. This is inherent in the present system due to the relatively small solid angle and the surface area of gas being used; these are imposed by the problem under investigation and the equipment presently available. Instead of electronic filtering, the traces were photographed, enlarged to 8 x 10, and hand-smoothed before amplitudes were read. These amplitudes, along with the appropriate calibrations, were reduced to T_m, T_{Br}, I_{λ_1}, I_{λ_2}, and k'_λ time profiles using a simple numerical iteration computer program.

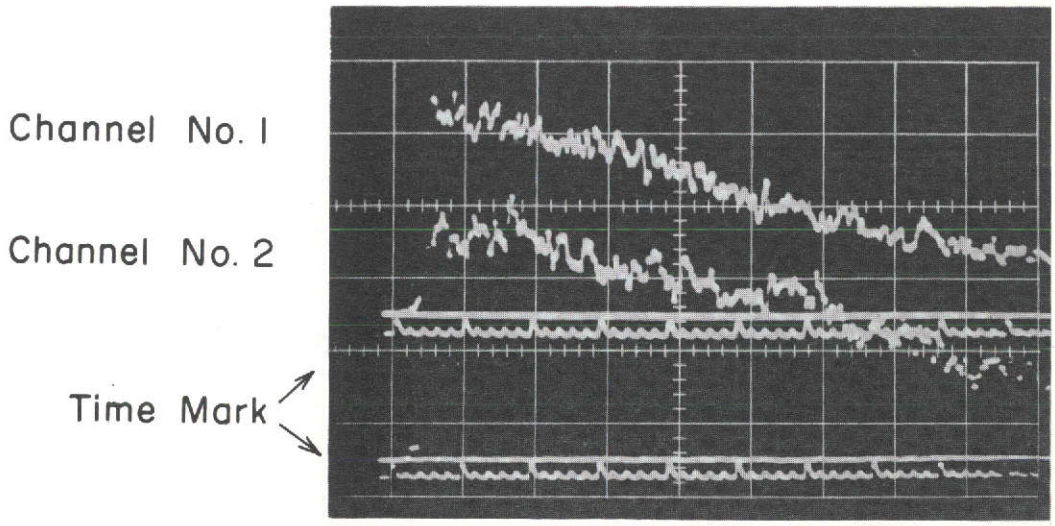

Fig. 9. Intensity Time-Histories for Channels 1 and 2 of DAIM System, Run No. 1752

The brightness and DAIM temperature measurements were performed in one of the two high performance shock-tubes existing at the O.S.U. Aeronautical and Astronautical Research Laboratory. This facility and its performance has been documented in the literature.[10,11] Briefly, the driver and driven sections are cylindrical with 10 cm inside diameters. The driver gas, helium at about 125 psig, is heated through an arc discharge process with the energy being supplied by a 11,000 μF capacitor bank. The energy stored in this bank is variable up to 200,000 J at 6000 V. The discharge occurs between the electrodes of a coaxial assembly which is recessed in the bottom of the driver section. The arc is initiated by an exploding wire between the electrodes, with the main bank discharge duration being approximately 80 μs for 90% energy dissipation. The energy transferred by the arc heating process increases the pressure and temperature of the driver gas. Three different volume drivers are available, the smallest volume having the highest energy density after discharge at a given voltage, thus, giving the strongest shock velocities. The small (mini-volume) and medium (midi-volume) size drivers were used in the present experiments.

The driver and the driven sections are separated by a prescored steel diaphragm which bursts due to the high pressure arc-heated driver gas and separates into six petals lying relatively flat against the shock-tube wall in a time span of approximately 200 μs.

The driven section, approximately 8.25 m long, is made of stainless steel. This section is connected through a 10 cm inside diameter valve to either a mechanical roughing pump or to an oil diffusion pump and mechanical roughing pump in series. The valve, when closed, preserves the contour of the shock-tube.

For the present tests, the driver section was evacuated to a few torr before being loaded with 125 psig helium. The driven section was pumped below 1×10^{-4} torr before each run and the leak rate at this pressure was considered acceptable if below 2×10^{-4} torr/min. These residual air pressures were measured with a number of instruments (McLeod Gage, CVC Phillips Cold Cathode Ionization Gage, and CVC VG1A Hot Cathode Ionization Gage) and their values agreed reasonably well.

The test gas used was synthetic air consisting of 79% nitrogen and 21% oxygen purchased through Air Reduction Company (Airco). In order to ensure a relatively pure sample of test gas, the shock-tube was purged once with synthetic air and then re-evacuated to below 1×10^{-4} torr before loading with the final test sample. For convenience in setting the initial pressure in the driven section, an auxiliary chamber of small volume (relative to the shock-tube) was loaded with the test gas sample at an intermediate pressure of 33.0 torr. When opened to the evacuated shock-tube, the resultant pressure of the combined system was the desired pressure of 1.00 torr. This intermediate pressure (auxiliary chamber pressure) was measured with a mechanical gage (Wallace and Tiernan 0 to 50 torr gage) and the filling system was calibrated using synthetic air and a cold-trapped

McLeod Gage for the final pressure measurement at 1.00 torr. The accuracy of the initial pressure setting (P_1) is thus determined by the accuracy of this initial calibration which is of the order of 1 to 2 percent.

The last 3.5 m of the driven section have observation ports every 0.5 m, each port consisting of a slit cut in the side of the tube with dimensions of 1.5 mm wide (along the shock-tube axis) by 14 mm high. Each slit is covered with a 1 mm thick synthetic sapphire window which is backed with an O-ring seal. The last three of these observation ports were used in making the shock velocity measurements, their distances from the endwall being 1.16, 0.66, and 0.16 m, respectively.

The hydrodynamic shock front and luminous (radiation) front can be considered coincident for the conditions of interest here. Thus, by measurement of the time between the arrival of the luminous front at two positions a known distance apart, an average velocity over the measured distance can be calculated. The distance between the two velocity ports was 0.5 m. Thus, with shock velocities from 7 to 10 km/s, the time to be measured is of the order of 50 μs or greater. In order to achieve a velocity measurement with an accuracy of ± 1%, the measurement system was designed to determine the shock transit time to within 0.5 μs.

The luminous front was monitored at each velocity point through a collimating system consisting of a pair of 0.4 mm wide slits 10 cm apart, the first slit being only a few centimeters from the shock-tube port. Thus, the field of view at the far side of the tube was approximately 1.5 mm wide. With shock velocities of 7 to 10 km/s the convection time (rise time) of this slit system is 0.25 μs or less.

The radiation passing through each velocity port collimating system was monitored with an RCA 931-A photomultiplier tube operated at 500 V with a linear voltage divider chain carrying 20 mA. To obtain the ultimate response time of the slit system and still maintain good signal levels, the photomultiplier tube outputs were fed through emitter follower circuits based on a design suggested by Menard.[12] These emitter followers possess an RC time constant of the order of 0.04 μs and enable the recording equipment to be located at a distance from the signal origin without degrading the response time of the present system. The output of the emitter follower circuits from the last two velocity ports were displayed on the upper and lower beams of a Tektronix 555 dual beam oscilloscope fitted with Type G plug-in units with both beams being driven with the lower time base. The external trigger of the upper time base of this oscilloscope was used to monitor the trigger photomultiplier tube (not possessing an emitter follower) and to pass a delayed triggering pulse to the lower time base. This delaying technique allows recording of the arrival of both luminous fronts, thus enabling a more accurate determination of the time between luminous fronts than a self-triggering system offers. In order to minimize sweep rate error, a time mark generator trace with 1- and 5-μs time marks was overlaid immediately before (or after) each run and was located at the bottom of each oscillogram channel, to improve reading accuracy.

V. RESULTS AND DISCUSSION

As indicated previously, the brightness and DAIM techniques have been applied to the time-resolved measurement of temperature behind reflected shock waves in air. The Ohio State arc-driven shock tube facility[10,11] was used for these measurements; the shock tube conditions covered included an initial driven tube pressure of 1 torr* and incident shock velocities ranging from 7 to 10 km/s.

Over twenty data points were obtained using the DAIM technique and with the shock tube being driven by the mini-driver (this is our smallest volume driver with a volume of 0.070 ft^3). Some of the results from these measurements are tabulated in Table 1. These measurements were obtained at a distance of 3.6 mm from the end-wall. Included in Table 1 for each run are the measured incident shock velocity, the predicted gas dynamic temperature (T_{gd}), the measured temperature at $t = 1$ μs after the reflected shock wave had passed the measurement position and based on the DAIM data reduction technique (T_m), the measured temperature at $t = 1$ μs based on interpreting channel 1 of the DAIM system as a brightness temperature (T_{Br}), the same two temperatures averaged over the first 5 μs after shock passage, and the optical thickness, $\tau_i = k'_\lambda \ell_1$, at $t = 1$ μs after shock passage. Although the test time at these shock tube conditions may be as much as 15-20 μs measured from the instant of shock reflection off the end wall,[13] it is felt that a conservative estimate is 10 μs. Since it takes the reflected shock wave nearly 4 μs to travel from the end-wall to the measurement position, then there should be at least 5 μs of data-taking time available before the test terminates, i.e., the reflected shock wave meets the leading edge of the contact region.

As may be seen from the data in Table 1, the measured DAIM temperatures are consistently higher than the predicted gas dynamic temperatures of Reference 14. This is illustrated in Fig. 10 where the measured DAIM temperatures at a time of $t = 1$ μs after reflected shock wave passage are compared with the gas dynamic temperature predictions of References 14 and 15.

The brightness temperature measurements, i.e., the interpretation of the channel 1 DAIM measurement as a brightness temperature, are shown in Fig. 11 and compared with the data of Fig. 10. These are all for a time of $t = 1$ μ after shock passage. As can be seen, at the lower shock velocities where the absorption is somewhat less, there is a larger deviation of the measured brightness and DAIM temperatures than at the higher velocities.

*Due to an error in pressure measurement some data were actually obtained at an initial driven tube pressure of 1.2 torr. These data show no consistent difference from the data obtained at 1 torr and, furthermore, the predicted gas dynamic temperature differs by only 1%.

Table 1 - Tabulation of Temperature Measurements Obtained With DAIM System Behind Reflected Shock Waves in Air, P_1 = 1 torr, x = 3.6 mm, Mini-Volume Driver

Run No.	U_s (km/s)	T_{gd} (K)	t = 1 μs		Averaged over t = 1-5 μs		Optical Thickness, τ_1, at t = 1 μs
			T_m, K	T_{Br}, K	T_m, K	T_{Br}, K	
1734	8.33	15,400	18,400	16,500	17,500	16,150	1.74
1735	8.47	15,650	18,250	16,650	17,750	16,400	1.91
1736	8.70	16,100	18,700	17,950	18,350	17,750	2.68
1737	8.77	16,250	18,750	17,000	18,450	16,850	1.87
1738	8.62	15,950	16,850	16,100	16,900	16,150	2.58
1739	8.40	15,550	17,050	16,000	16,800	15,850	2.21
1740	8.70	16,100	17,700	17,050	17,600	16,950	2.73
1741	9.09	16,800	19,450	18,900	18,850	18,450	3.12
1742	8.85	16,400	17,700	17,300	17,700	17,300	3.30
1743	9.26	17,100	19,250	18,950	19,100	18,850	3.66
1744	9.43	17,350	19,550	19,050	19,250	18,750	3.11
1745	9.09	16,800	19,150	18,400	18,750	18,100	2.76
1746	9.43	17,350	18,250	18,000	18,150	17,900	3.74
1749	9.62	17,700	19,300	19,000	18,850	18,600	3.58
1750	9.43	17,350	19,300	18,750	18,800	18,350	3.01
1752	9.52	17,500	19,150	18,850	18,750	18,500	3.58
1753	8.20	15,150	16,750	15,050	16,350	14,850	1.71
1754	8.47	15,650	17,200	16,050	16,800	15,800	2.13
1755	7.63	13,800	16,450	11,800	15,850	11,600	0.72
1756	7.63	13,800	15,450	11,750	15,000	11,600	0.85
1757	7.94	14,600	15,800	13,450	15,800	13,450	1.33
1758	8.13	15,000	15,950	14,650	16,000	14,550	1.90
1759	7.81	14,300	15,000	12,900	14,450	12,650	1.34
1760	8.00	14,700	15,950	13,100	15,350	13,000	1.15

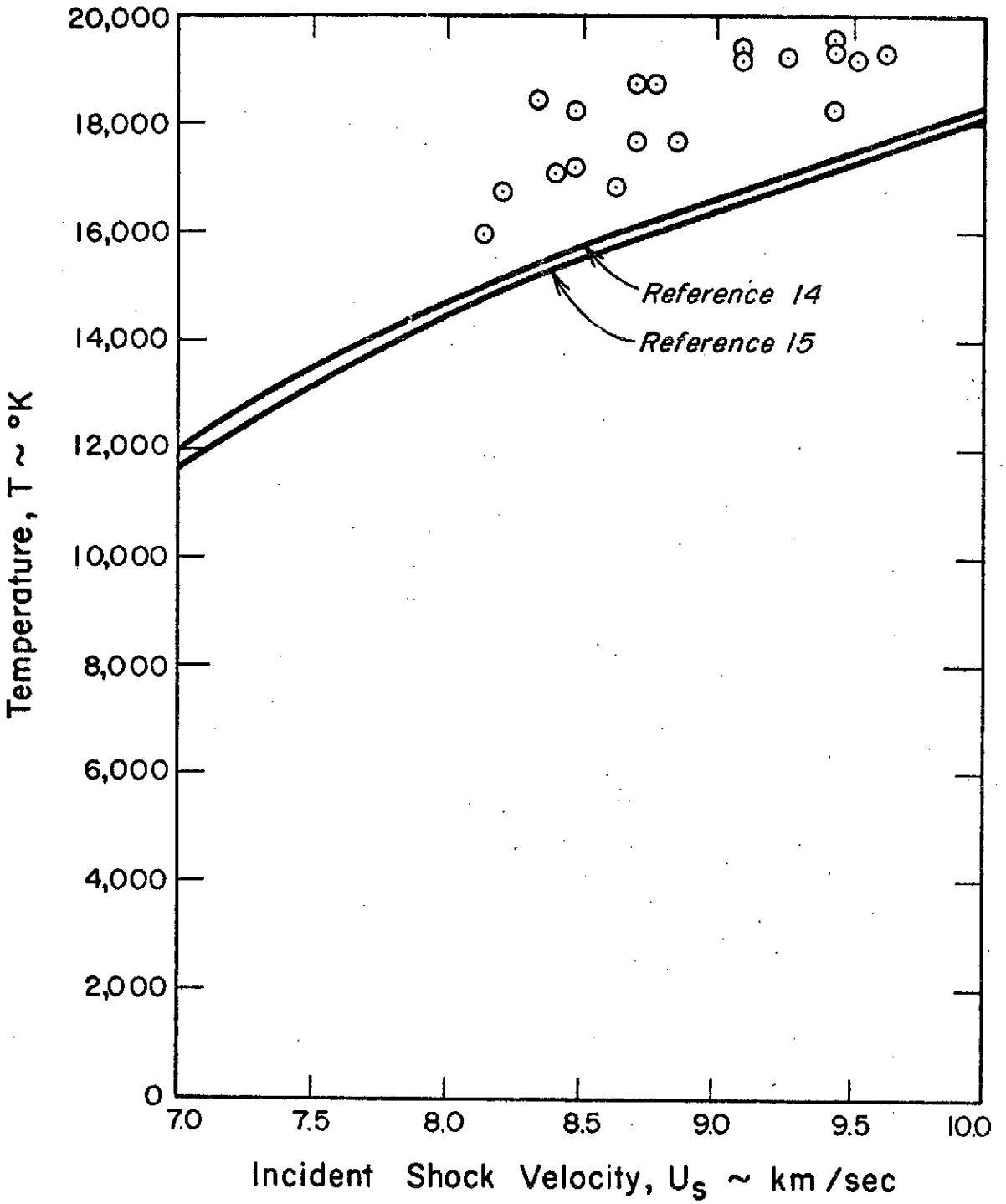

Fig. 10. DAIM Temperatures at t = 1 μs After Passage of Reflected Shock Wave as a Function of Incident Shock Wave Velocity, P_1 = 1 torr, x = 3.6 mm, Mini-Volume Driver Used

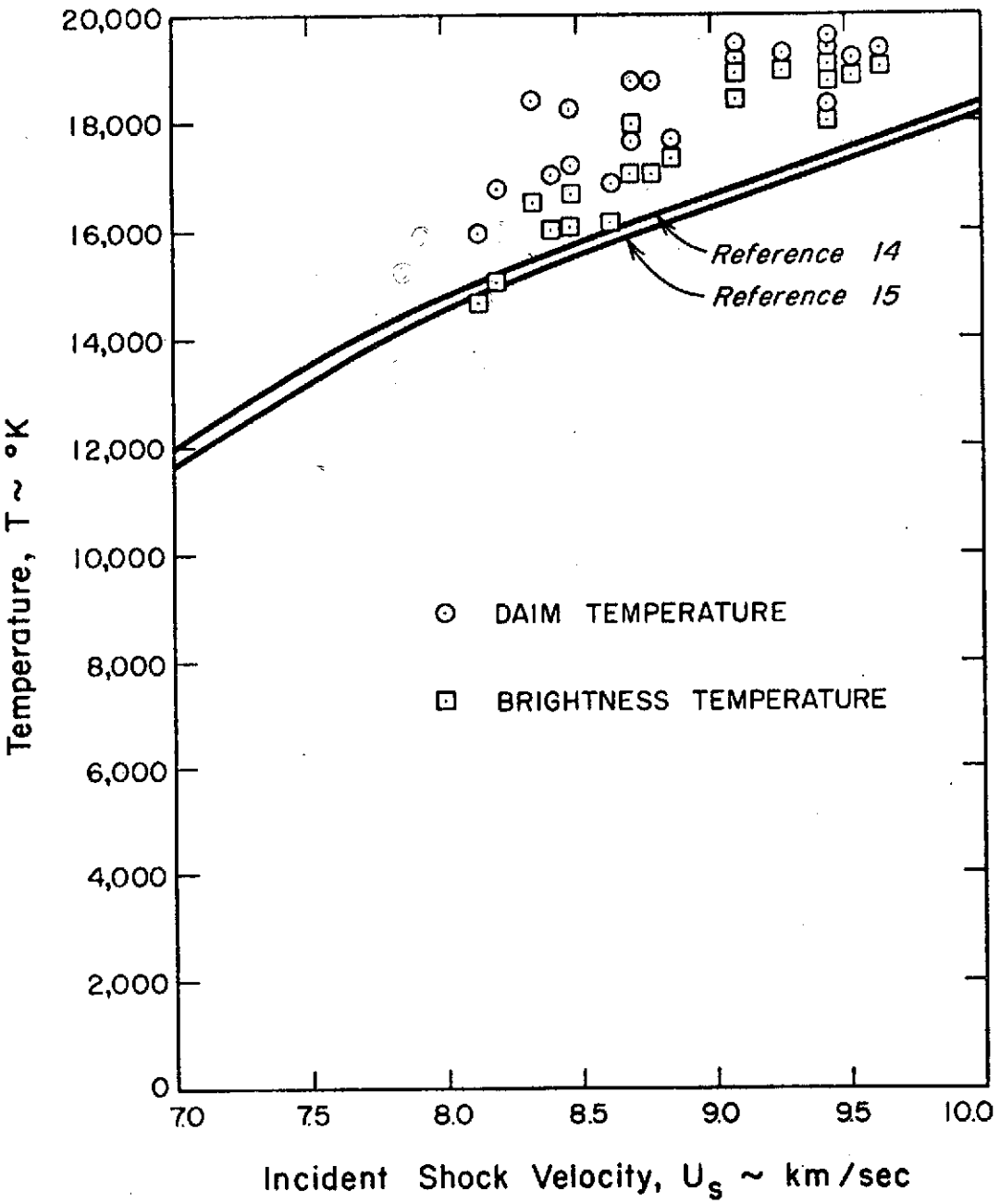

Fig. 11. Comparison of Brightness Temperature Measurements (Channel 1 of DAIM System) and DAIM Temperature Measurements, t = 1 μs After Shock Passage, P_1 = 1 torr, x = 3.6 mm, Mini-Volume Driver Used

The fact that the test gas absorption coefficient does increase with increasing shock velocity is shown in Fig. 12. Here the gas absorption coefficient, at a time of t = 1 μs after shock passage and based on the ratio of the intensities from the two DAIM channels using Fig. 6, is presented as a function of incident shock velocity. In Fig. 13, representative absorption coefficient time-histories are presented. Again, the increase in the magnitude of the absorption coefficient with increasing shock velocity is apparent. As may also be seen, however, there is no major variation in the absorption coefficient with time for a time period of 15 μs or more.

Since the path length for channel 1 was 10 cm, the associated optical thickness τ_1 was of the order of 3 at the higher velocities, and the brightness and DAIM temperatures in Fig. 11 are seen to be in good agreement at these conditions. At lower velocities, τ_1 was of the order of 1. Although data were taken at incident shock velocities as low as 7.5 to 8.0 km/s, no temperature data has been presented graphically for conditions where τ_1 is less than 1.5. This is because, when τ is small, the measured temperature becomes extremely sensitive to the specific value of τ deduced from the data and the accuracy of the measurement becomes severely degraded.

It should be noted that the brightness temperature, which is based on the assumption that the gas radiates as a blackbody, represents a lower limit on the gas temperature. If the gas is not a blackbody, then the actual gas temperature (at least somewhere along the optical path) must be higher than the measured brightness temperature. It is apparent in Fig. 11 that at the higher incident shock velocities, the measured brightness temperatures lie above the predicted gas dynamic temperature. Since these measured brightness temperatures do represent a lower limit on the gas temperature, this is a further indication of the deviation between the present data and the predicted gas dynamic temperatures.

A further illustration of this point is contained in Fig. 14 where the measured temperature is graphed as a function of the predicted gas dynamic temperature. This, again, is for a time of 1 μs after shock passage. Figure 14 shows the temperature data to be approximately 10 percent higher than the predicted values. An error analysis is shown in Table 2 and shows the possibility of a 5 percent systematic bias error and a 7 percent random error. This error analysis is in terms of the intensity, and for S ranging from 1 at the lower shock velocities to 2 at the higher velocities (see Figs. 2, 4, and 5), the temperature measurement error would range from 5 percent bias and 7 percent random at the lower shock velocities to 2.5 percent bias and 3.5 percent random at the higher velocities. This obviously is not sufficient to explain the deviation apparent in Fig. 14, since the systematic bias error and the random error would not be linearly additive.

Furthermore, the present results are not in agreement with that of earlier investigators who also found their temperature measurements to consistently deviate from the predicted gas dynamic values, but in

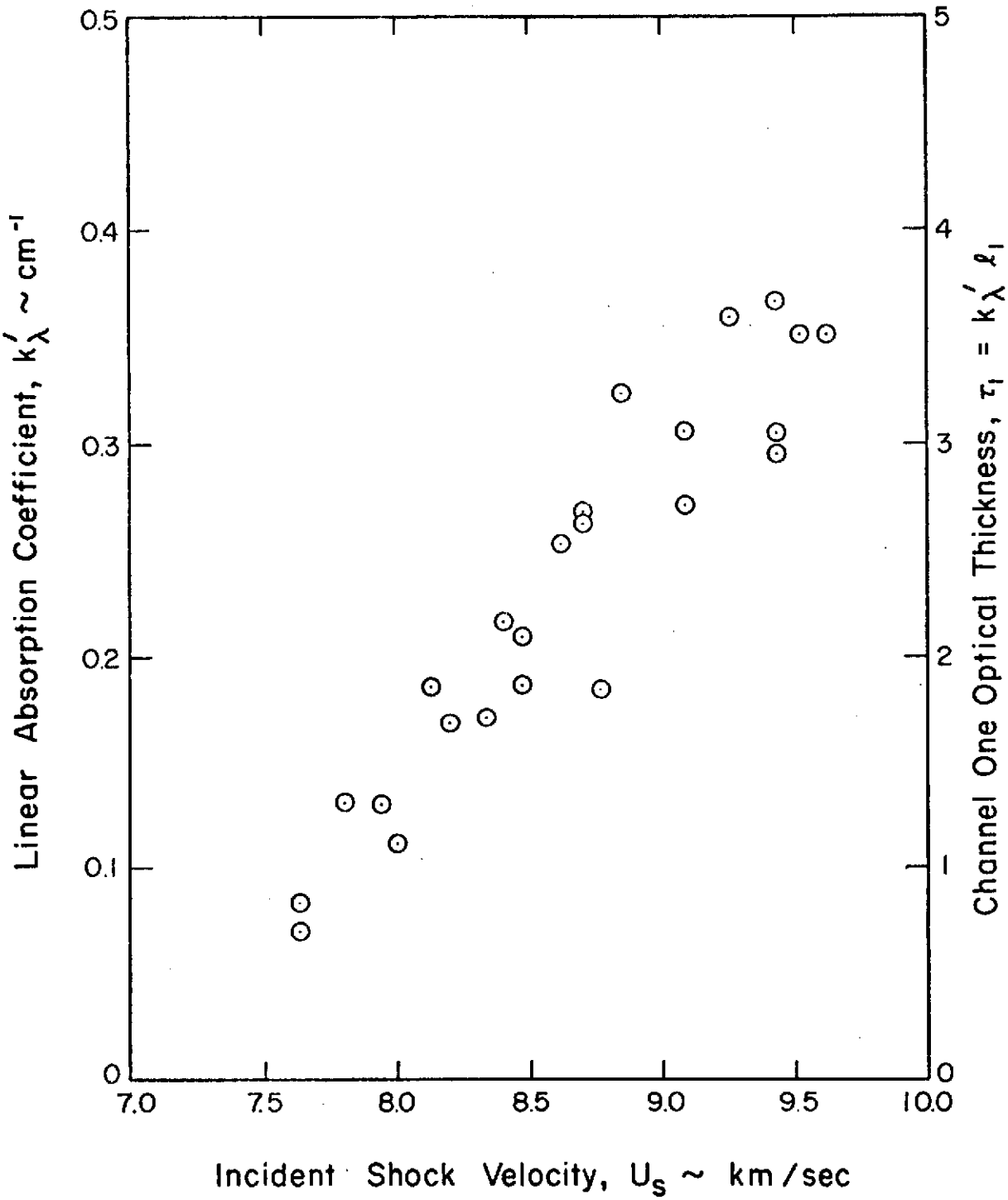

Fig. 12. Measured Absorption Coefficient, k'_λ, and Optical Thickness (based on shock tube diameter), τ_1, as a Function of Incident Shock Velocity, t = 1 μs After Shock Passage, P_1 = 1 torr, x = 3.6 mm, Mini-Volume Driver Used

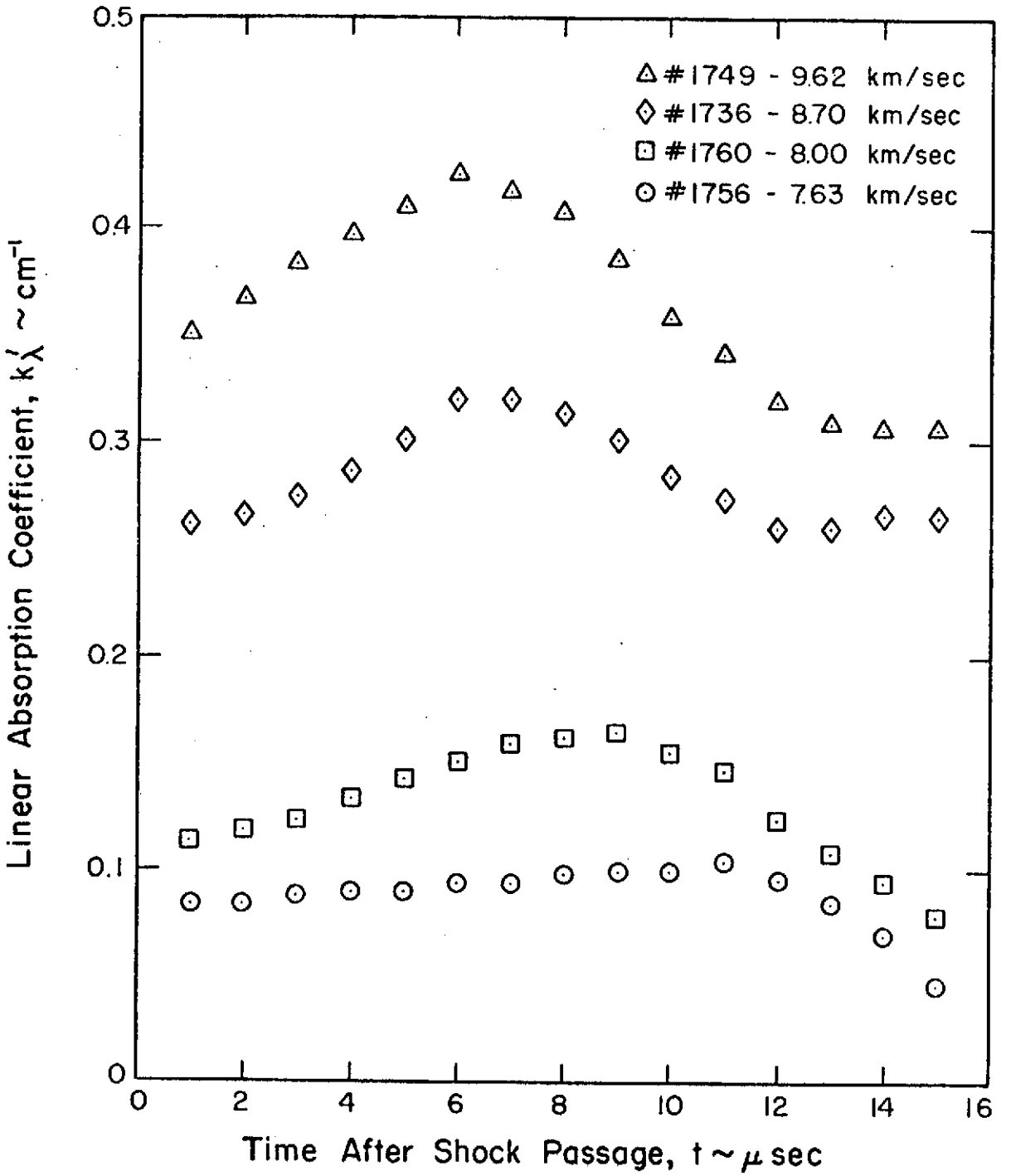

Fig. 13. Measured Absorption Coefficient Time-Histories, P_1 = 1 torr, x = 3.6 mm, Mini-Volume Driver Used

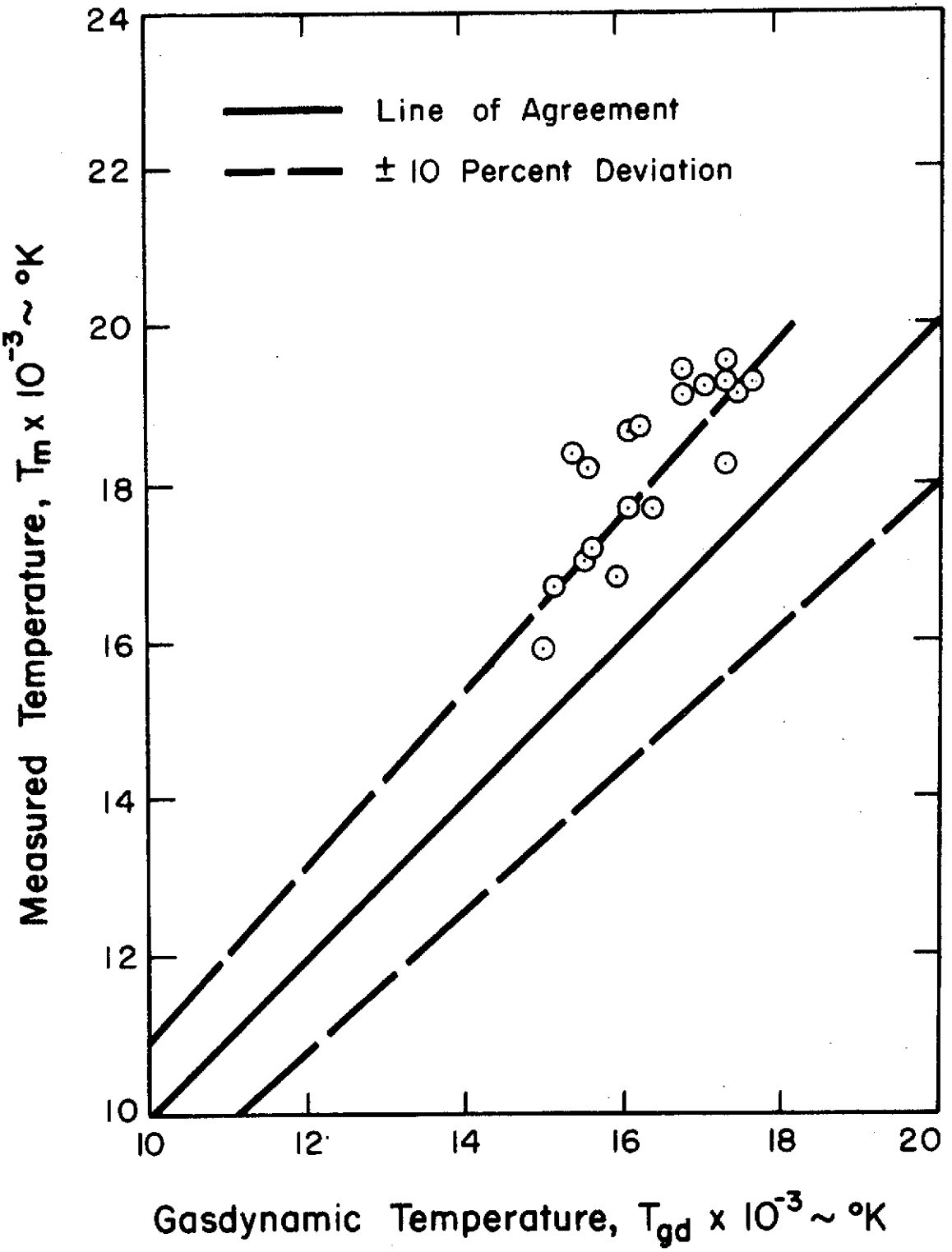

Fig. 14. Measured DAIM Temperature Versus Predicted Gas Dynamic Temperature from Reference 14, t = 1 μs After Shock Passage, P_1 = 1 torr, x = 3.6 mm, Mini-Volume Driver Used

Table 2 - Error analysis for DAIM System Intensity Measurements

Source of Error	Estimated Percent Error	
	Bias	Random
1. Ribbon Filament Lamp		
NBS Lamp	± 2	
Eppley Lamp		± 1
Ratioing of Lamps		± 1
2. Calibration Using Keithley 414	± 1	± 1
3. Window Transmissivity (80% of Window Samples in this range)		± 1
4. Oscilloscope Calibration		± 1
5. Signal to Noise Ratio		± 2
6. Linearity of Photomultiplier	± 2	
TOTAL ESTIMATED ERROR	± 5	± 7

the opposite direction. Wood and Wilson,[1,2] using air seeded with hydrogen and also making measurements behind reflected shock waves, found their measured temperatures to be on the average 5-6 percent lower than their predictions. This was for an initial driven tube pressure of 0.2 torr and for post-reflected shock wave temperatures ranging from 10,000 to 16,000 K. Bengston et al.[3] in a similar study, but using neon with small amounts of spectroscopic additives, found their measured temperatures to be on the average 3 percent lower than the predictions.

It should be emphasized that to the authors' knowledge extreme care was taken in all three of these experimental investigations to account for the various factors which enter in. For example, in the present work a d.c. calibration was made of both the oscilloscopes used and the Keithley 414 micro-microammeter using an IBI Model 600 d.c. potentiometer and a variable current source. The time marker was also compared with a standard. Checks were made for light leaks and for reflections off of slits or windows that would allow stray light to re-enter the optical train. In addition, the ribbon lamp filaments were scanned to locate the presence of hot spots and to determine the magnitude of the intensity gradient along the filament. The possibility of photomultiplier fatigue was tested at the calibration intensity used in the experiments (there was no evidence of such fatigue). Finally,

checks were made on the photographic enlargement and development techniques. As a result, it is felt that the differences between the data and predicted gas dynamic temperatures shown in Fig. 14 are not due to experimental technique.

This anomaly between the measured temperatures and the predicted values is further compounded when one looks at the measured temperature time-histories which are shown for selected cases in Figs. 15 (a)-(c). In these figures, the runs have been grouped according to incident shock velocity. Although there is reasonable agreement between repeated runs at the same approximate shock velocity, there is, in general, a fall off in measured temperature with time measured from the instant of shock passage. This was expected at the higher shock velocities, e.g., Fig. 15(c), where radiative cooling was expected to make its presence felt. The data at these higher velocities does, in fact, agree reasonably well with the predicted decrease in temperature from the radiative-gas dynamic coupled reflected shock wave flow field calculations by Nerem et al.[16,17], which used a five-step absorption coefficient model.[18] However, a somewhat similar trend also exists at lower shock velocities. This is not so easily explained since at incident shock velocities below 8.25 km/s radiative cooling effects are predicted to be negligible. It must be noted, though, that assuming the measured temperatures are correct, then the fact that they are elevated by, on the average, 10 percent would result in a more pronounced radiative cooling effect. On the other hand, at these lower velocities τ_1 is less than 1.5 and the associated accuracy of the DAIM measurement makes it impossible to conclude anything about any temperature variation with time behind the reflected shock front.

There are other factors which must be considered in the interpretation of the data. There is the possibility of a chemical nonequilibrium effect which might evidence itself both in the incident shock-heated gas as well as behind the reflected shock wave. With regard to the latter, the measurements and calculations of Nerem et al.[19] indicate that relaxation to chemical equilibrium (to within 1% in terms of temperature) would occur within 1-2 μs after reflected shock passage at a shock velocity of 7 km/s and within much less time at the higher velocities of this study. Thus, although slightly enhanced temperatures might be expected in the post-shock nonequilibrium region, its limited extent suggests that any effect would be negligible and would not influence the interpretation of the observations reported here.

With regard to any post-incident shock nonequilibrium effect on the present measurements, the radiative relaxation distance (intensity approaches to within 10% of the equilibrium intensity) behind an incident shock traveling 7.5 km/s in air at 1 torr would be less than 1 centimeter.[17] Although relaxation to within 1 percent on temperature would require a distance an order of magnitude longer, any effect due to the slight nonequilibrium in this region would be expected to be removed by the rapid post-reflected shock relaxation. Thus, here also, it is

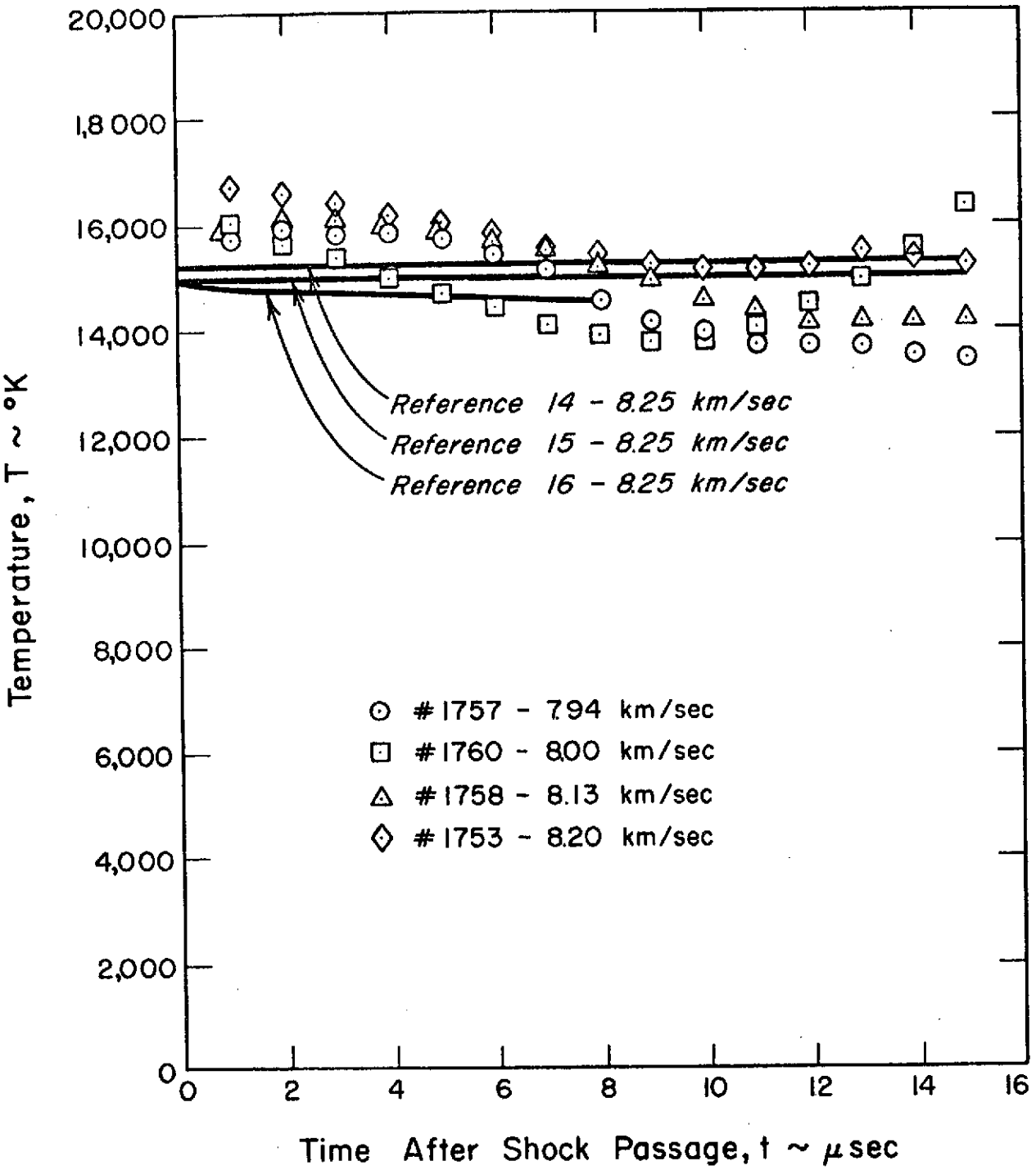

Fig. 15. Measured DAIM Temperature Time-Histories, P_1 = 1 torr, x = 3.6 mm, Mini-Volume Driver Used:

(a) $7.94 \leq U_s \leq 8.20$ km/s

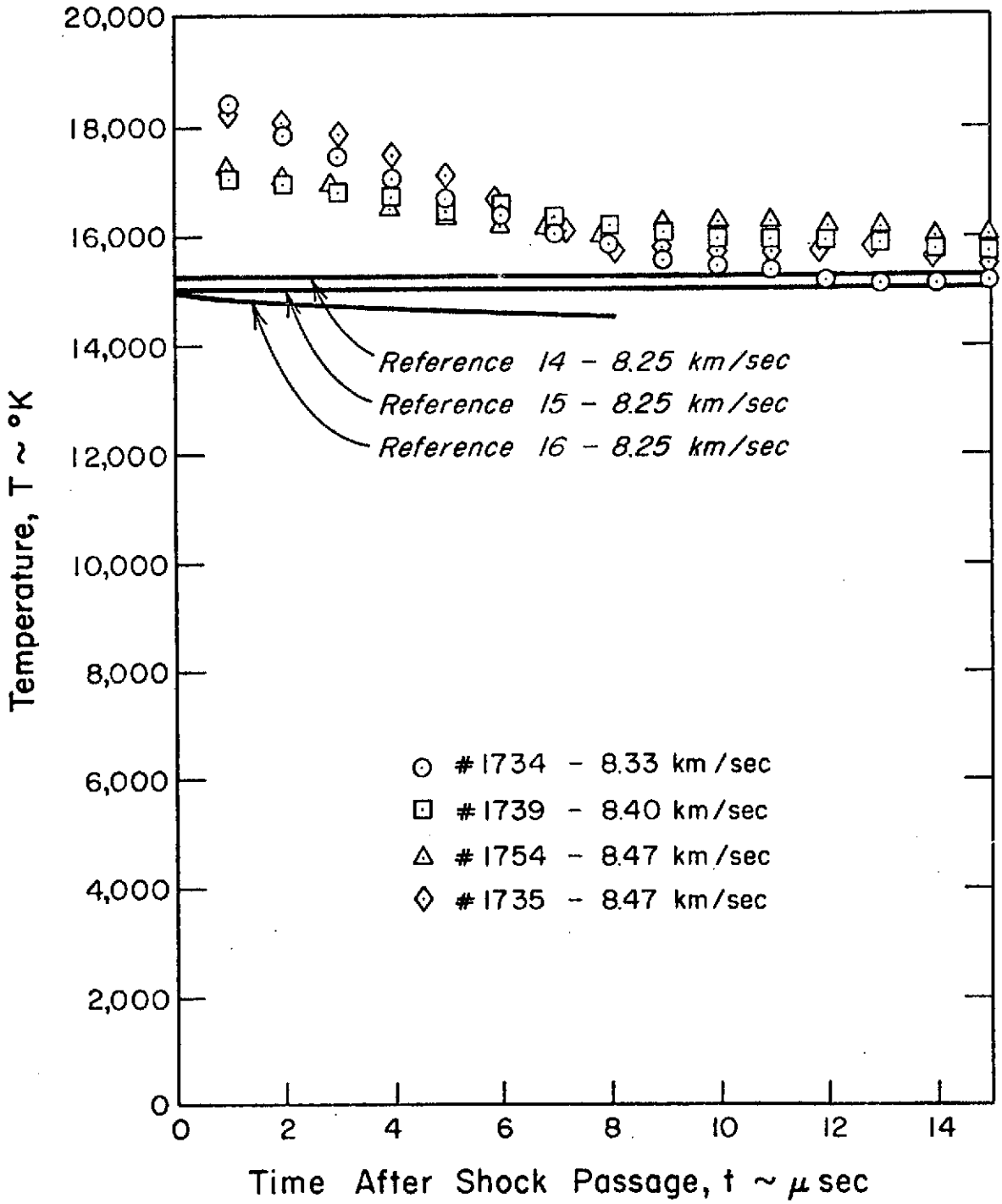

Fig. 15 (continued)

(b) $8.33 \leq U_s \leq 8.47$ km/s

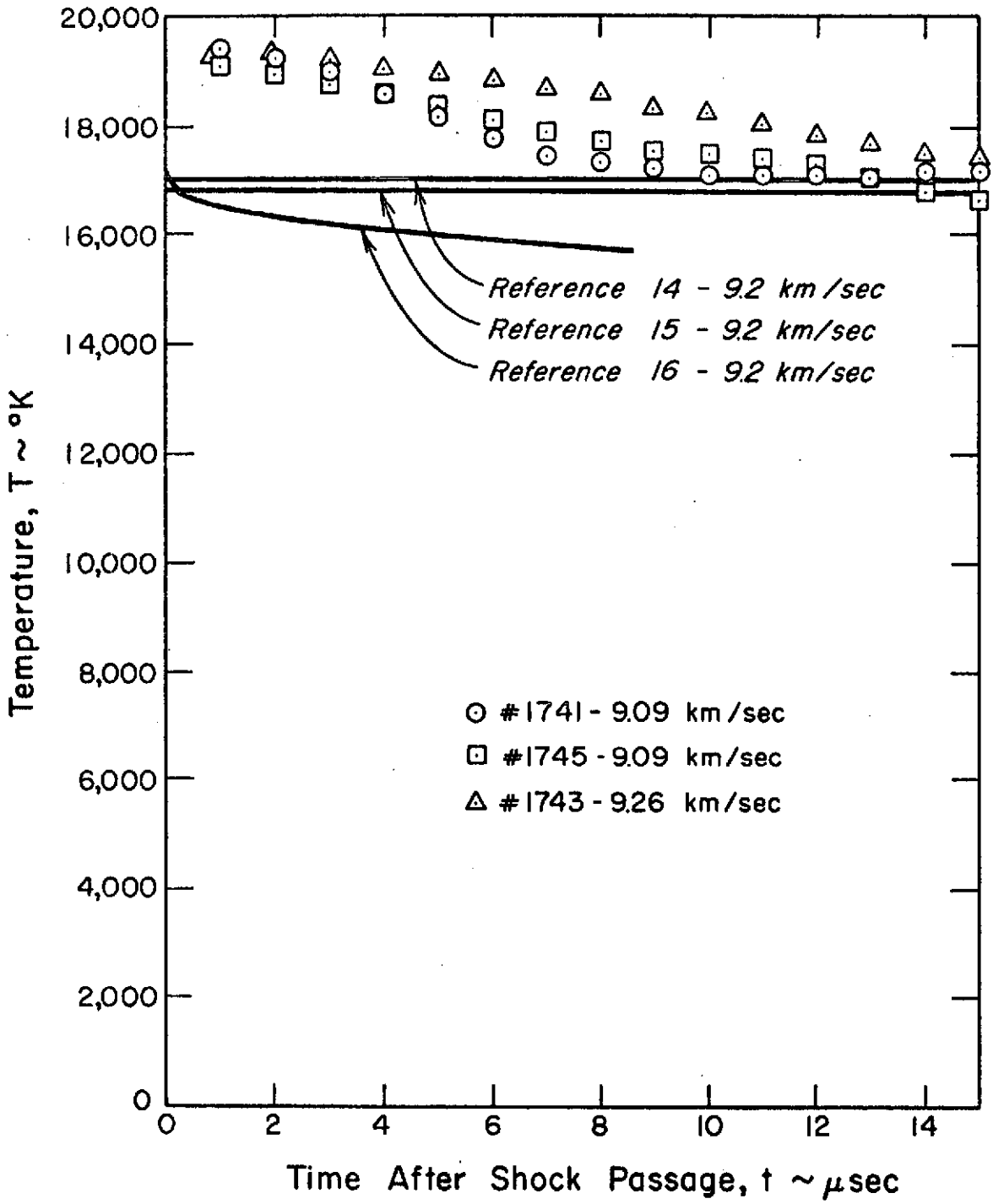

Fig. 15 (continued)

(c) $9.09 \leq U_s \leq 9.26$ km/s

concluded that any nonequilibrium effect on the interpretation of the present data is not important.

Another factor which should be noted is the reflected shock velocity time-histories measured by R. C. Prior and reported in Reference 20. These show that as the reflected shock wave leaves the end-wall it will first decelerate (the measured initial attenuation rate agrees quite well with the predicted radiative cooling effect by Nerem et al.[16,17]) and then accelerate. The time after shock reflection at which this acceleration begins increases with increasing incident shock velocity; presumably, because the radiation is stronger at the higher velocities and thus, the radiation induced attenuation dominates for a longer period of time. For incident shock velocities below 9 km/s, radiation effects are small and the acceleration begins almost immediately. Although this behavior has been observed by others[21,22] and is believed to be associated with the interaction of the reflected shock wave with the side wall boundary layer, it has not been satisfactorily explained from a theoretical viewpoint. Prior's measurements do, however, indicate an acceleration rate of 10^5 km/s^2. Since the reflected shock speed is of the order of 1 km/s, an appreciable change in reflected shock velocity could result in a few microseconds. This would be accompanied by an increase in the post-shock temperature, and would possibly influence the temperature time-histories observed in the present experiments.

Equally critical in the interpretation of the present data is the possible effect of axial gradients in the incident shock heated gas. These gradients could be the result of shock attenuation or, equally well, the effect of the side wall boundary layer. Mirels[23] has analyzed such boundary layer growth effects and has carried out calculations of the resulting influence on the flow properties. In essence, because of the side wall boundary layer growth, the flow behind the incident shock wave decelerates (relative to the shock wave) and the pressure, density, and temperature increase. Although the temperature behind the incident shock wave is predicted to increase by only a few percent as one proceeds towards the contact surface, this effect becomes magnified when this post-incident shock flow is further shock-heated, e.g., by a standing or reflected shock wave. Thus, in the worse case, the post-reflected shock wave temperature may be increased by as much as 10 or even 20 percent.

Such boundary layer effects are most pronounced when the length of the test gas slug approaches its maximum value, as may be seen from the results of Reference 23. Since, for the present experiments, the test gas slug was of the order of 80-90 percent of its maximum length, the presence of side wall boundary layer effects cannot be ruled out. In addition, if one assumes that a reflected shock wave moving into such a side-wall boundary layer influenced region will adjust its speed so as to stagnate the gas it processes, then the reflected shock wave velocity would be expected to increase as it moved away from the end-wall. This would further accentuate the magnification of the temperature,

and produce an increasing post-reflected shock temperature with distance from the end-wall, which would be consistent with the observations of Prior.[20]

In order to explore whether or not such an effect did, in fact, manifest itself, a limited number of additional measurements were carried out at a distance of only 1.6 mm from the end wall. Theoretical calculations indicate that even this close to the end-wall the observed region will be outside the end-wall boundary layer during the data taking period.[16,17] These data are presented in Table 3 and in Fig. 16 where they are compared with the previous data of Fig. 10. As can be seen, the data obtained at 1.6 mm from the end-wall lie on the lower side of the scatter of the data obtained at 3.6 mm from the end-wall and are in much better agreement with the predicted gas dynamic temperatures. Although the data at the 1.6 mm position are limited in quantity, they suggest that there may be a gradient in post-reflected shock wave temperature which would be consistent with a sidewall boundary layer effect.

It should be noted that, because of the much larger X/D (driven tube length/diameter) ratio associated with the present experiments as compared with the earlier studies of Wood and Wilson[1,2] and Bengston et al.,[3] such a boundary layer effect would be expected to be more severe in the present situation. This might at least partially account for the higher temperatures observed here (on the average approximately 10 percent above theory) as compared to References 2 and 3 (6 and 3 percent low, respectively).

Furthermore, such a boundary layer effect might also explain why, for comparable conditions (8-10 km/s, P_1 = 0.2 torr in Reference 2, and 7-10 km/s, P_1 = 1.0 torr in the Ohio State studies), radiative cooling effects have not been observed behind reflected shock waves in the Lockheed experiments while they have been in these studies. The slightly higher temperatures measured at Ohio State would result in the earlier onset of radiative cooling effects and, thus, a more pronounced effect for a given incident shock velocity.

Another boundary layer effect which may be important is an apparent shortening of the path length for each of the two DAIM channels due to the presence of wall boundary layers (both the shock tube side-wall boundary layer and that on the splitter). This effect is caused by the relative transparency of these cooler wall layers and can be approximately accounted for by shortening the path length by a distance equal to the sum of the two wall boundary layer thicknesses. As an example of the magnitude of this effect, the temperature resulting from the measured intensities for Run No. 1753 (see Table 1), assuming a boundary layer 2 mm in thickness is present on both the sidewall and the splitter, is 16,050 K. This is for a time of t = 1 μs after shock passage and should be compared to a temperature of 16,750 K from Table 1. A 2 mm boundary layer thickness is not unreasonable[24] and, thus, the temperatures

Table 3 - Tabulation of Temperature Measurements Obtained With DAIM System Behind Reflected Shock Waves in Air, P_1 = 1 torr, x = 1.6 mm, Mini-Volume Driver

Run No.	U_s (km/s)	T_{gd} (K)	t = 1 μs		Averaged over t = 1-5 μs		Optical Thickness τ_1, at t = 1 μs
			T_m, K	T_{Br}, K	T_m, K	T_{Br}, K	
1763	8.47	15,650	16,300	15,250	16,100	15,050	2.15
1764	9.35	17,200	18,700	18,500	18,450	18,200	3.95
1765	8.33	15,400	16,000	14,900	15,850	14,750	2.06
1766	9.17	16,950	18,400	18,050	18,500	18,150	3.50

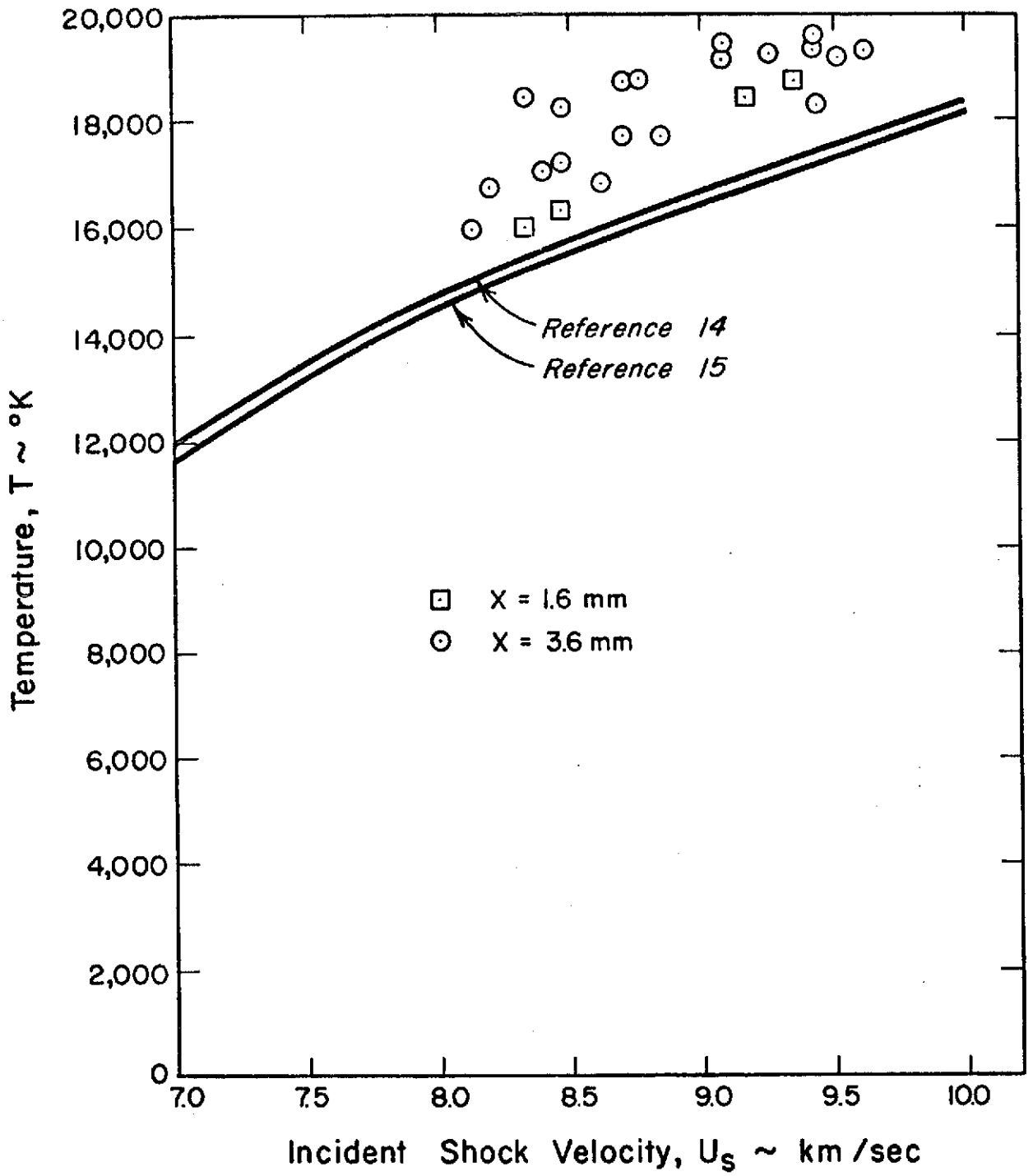

Fig. 16. Comparison of DAIM Temperature Measurements Obtained at 1.6 mm and 3.6 mm from End Wall, t = 1 μs After Shock Passage, P_1 = 1 torr, Mini-Volume Driver Used

reported here should possibly be somewhat lower due to this boundary layer effect.

Run No. 1753 is for a relatively low incident shock velocity. At higher shock velocities where τ is larger, $T_m \simeq T_{Br}$ and boundary layer absorption may be important. In this case, the effect of the boundary layer should be such that the data reduction will yield too low a temperature. In any event, it is clear at this point that boundary layer effects may be important and should be investigated further. Unfortunately, time limitations prevent us from doing this.

As a further and final check on the application of the DAIM technique, a second series of measurements were carried out using our medium-size driver chamber. This is the so-called midi-driver which has a volume of 0.081 ft^3 and which has been used in a majority of our previous studies, e.g. Reference 13. This driver and the mini-driver used in measurements reported in Table 1 are very similar, having the same coaxial electrode arrangements, and volumes which are approximately the same. However, the electrodes are closer to the diaphragm in the mini-driver, and as has been noted and is apparent in Fig. 17, the driver gas coming down the tube after the contact surface radiates much more strongly when the mini-driver, rather than the midi-driver, is used. This is assumed to be associated with an increased amount of driver gas contamination in the contact region due to the proximity of the electrodes and has been borne out by time-resolved spectroscopic measurements.[25]

Some of the results obtained with the midi-driver are presented in Table 4 and representative temperature time-histories are shown in Fig. 18(a)-(b). These results, for a time of $t = 1$ μs after shock passage, are compared in Fig. 19 with the previous data of Fig. 10. As may be seen, the data obtained with the midi-driver lies rather consistently on the low side of the general scatter of data from Fig. 10 for the mini-driver. This is further illustrated in Fig. 20 where the measured temperatures are graphed as a function of the predicted gas dynamic temperature. Here the data are seen to deviate on the average only 5 percent from the predictions as compared to the 10 percent deviation obtained with the mini-driver. This now places the deviation approximately within the accuracy of the experimental measurement (see Table 2).

It is interesting, in some ways strange, that there should result this difference between data obtained using two drivers so nearly alike. The reason for this is certainly not understood, even though there are the previously noted observational differences in driver gas radiation (see Fig. 17). However, it does point out a possible problem, not only in this facility, but also in other facilities.

In terms of the application of the technique itself, in many shock-tube studies a 10 percent accuracy temperature would be considered more

Table 4 - Tabulation of Temperature Measurements Obtained With DAIM System Behind Reflected Shock Waves in Air, P_1 = 1 torr, x = 3.6 mm, Midi-Volume Driver

Run No.	U_s (km/s)	T_{gd} (K)	t = 1 μs		Averaged over t = 1-5 μs		Optical Thickness, τ_1, at t = 1 μs
			T_m, K	T_{Br}, K	T_m, K	T_{Br}, K	
1768	8.62	15,950	17,700	16,400	17,150	16,050	2.07
1769	8.62	15,950	16,150	15,250	16,400	15,300	2.30
1770	9.01	16,650	17,750	17,250	17,350	16,900	3.03
1771	7.75	14,150	19,150	13,650	16,550	13,050	0.77
1773	8.00	14,700	17,200	14,900	17,000	14,750	1.45
1774	8.33	15,400	16,350	14,900	16,400	14,900	1.83
1775	8.33	15,400	17,000	15,200	16,350	14,850	1.68
1776	8.70	16,100	17,850	16,600	17,250	16,350	2.09
1777	8.62	15,950	16,450	15,800	16,150	15,650	2.68
1778	8.93	16,500	17,350	16,900	17,100	16,700	3.09
1779	9.01	16,650	17,950	17,300	17,600	17,100	2.81
1780	9.09	16,800	18,250	17,800	18,050	17,650	3.16
1781	8.62	15,950	16,950	16,300	16,850	16,200	2.67
1782	8.70	16,100	16,750	16,200	16,700	16,050	2.79
1784	8.85	16,400	17,600	16,950	17,350	16,750	2.68

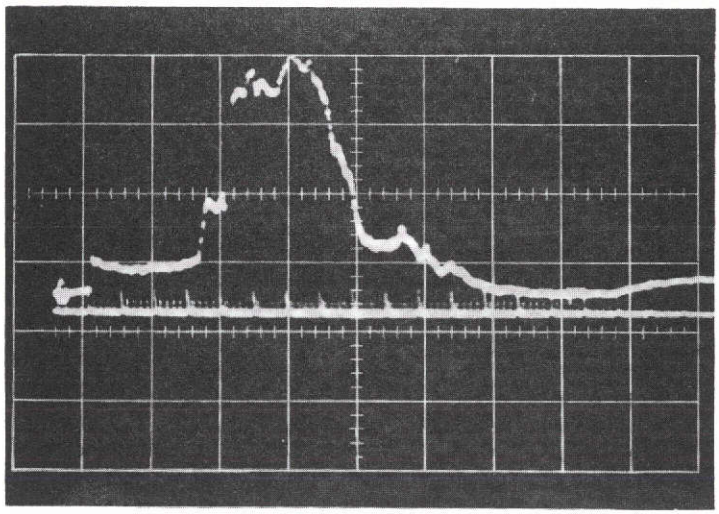

(a) Run No. 1763, U_s = 8.47 km/sec
Mini - Volume Driver

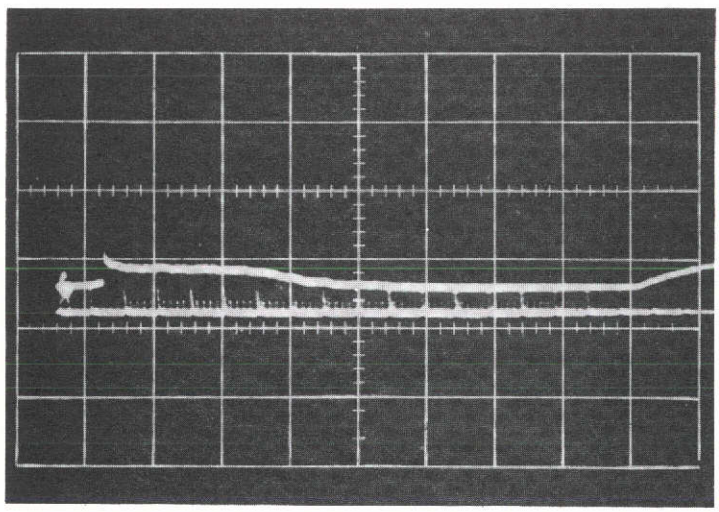

(b) Run No. 1774, U_s = 8.33 km/sec
Midi - Volume Driver

Fig. 17. Comparison of Time-Resolved Incident Shock Wave Broad Band Radiative Intensity Measurements Showing Differences in Driver Gas Radiation for Mini-Driver and Midi-Driver

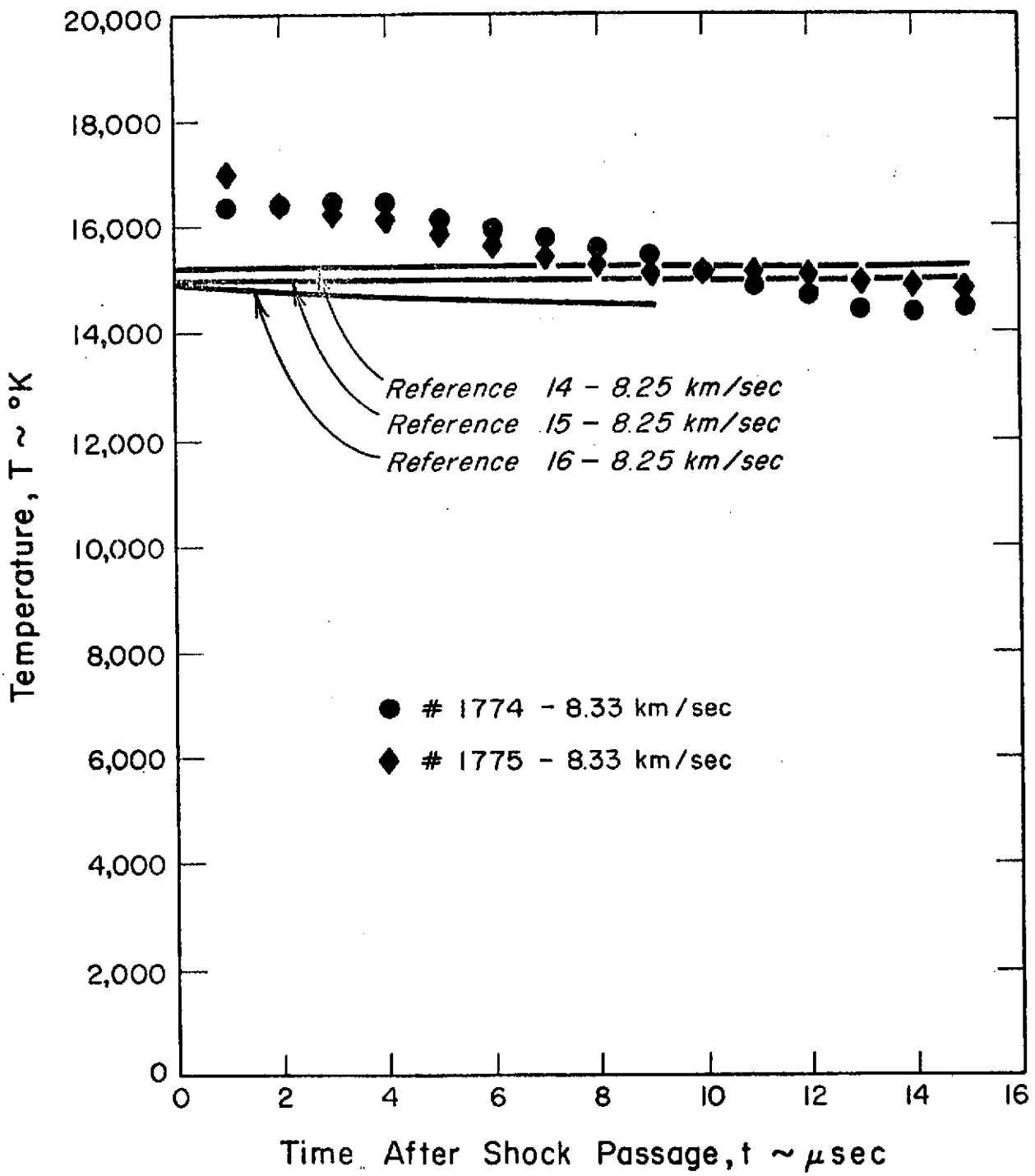

Fig. 18. Measured DAIM Temperature Time Histories, P_1 = 1 torr, x = 3.6 mm, Midi-Volume Driver Used:

(a) U_S = 8.33 km/s

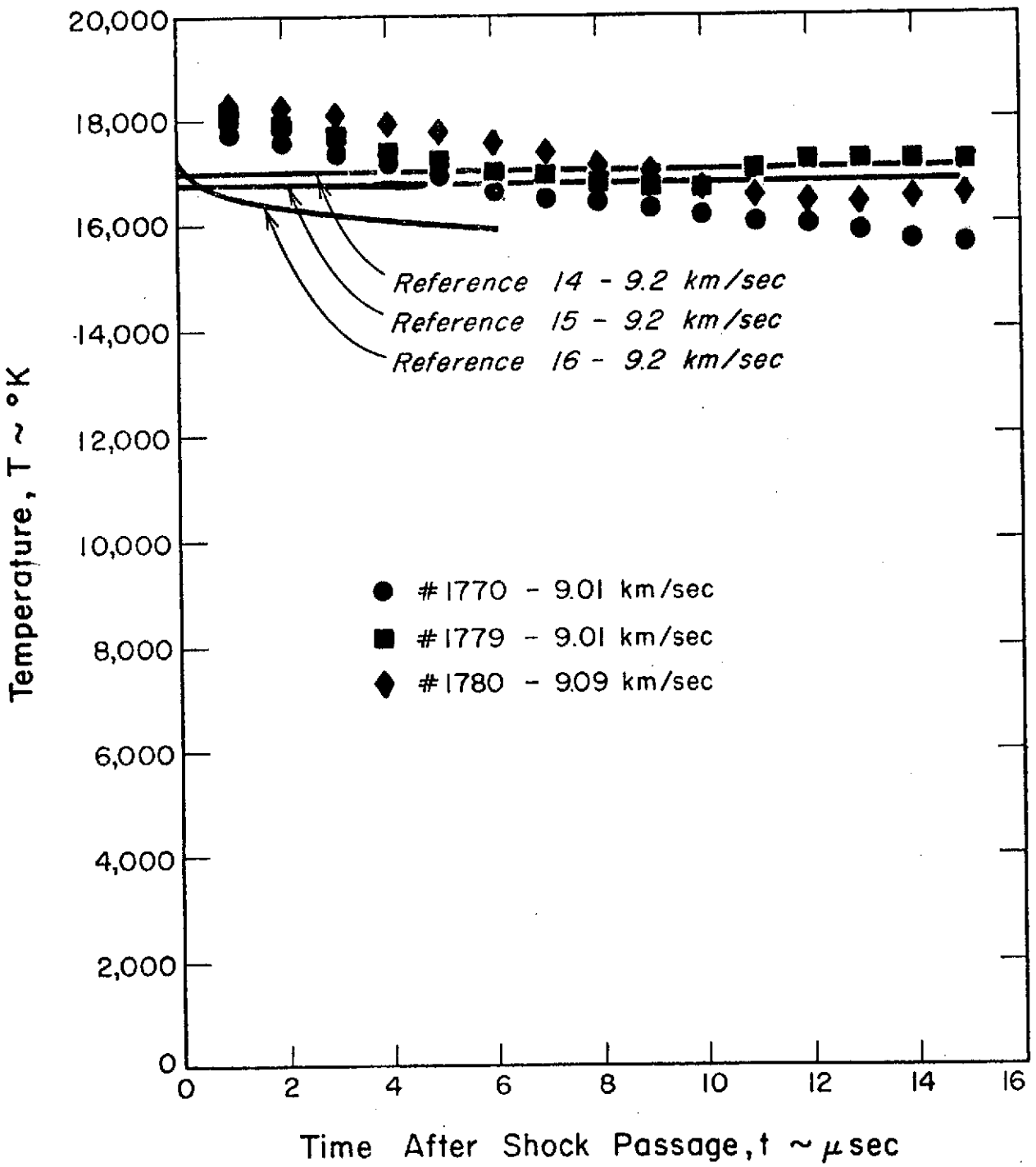

Fig. 18 (continued)

(b) $9.01 \leq U_s \leq 9.09$ km/s

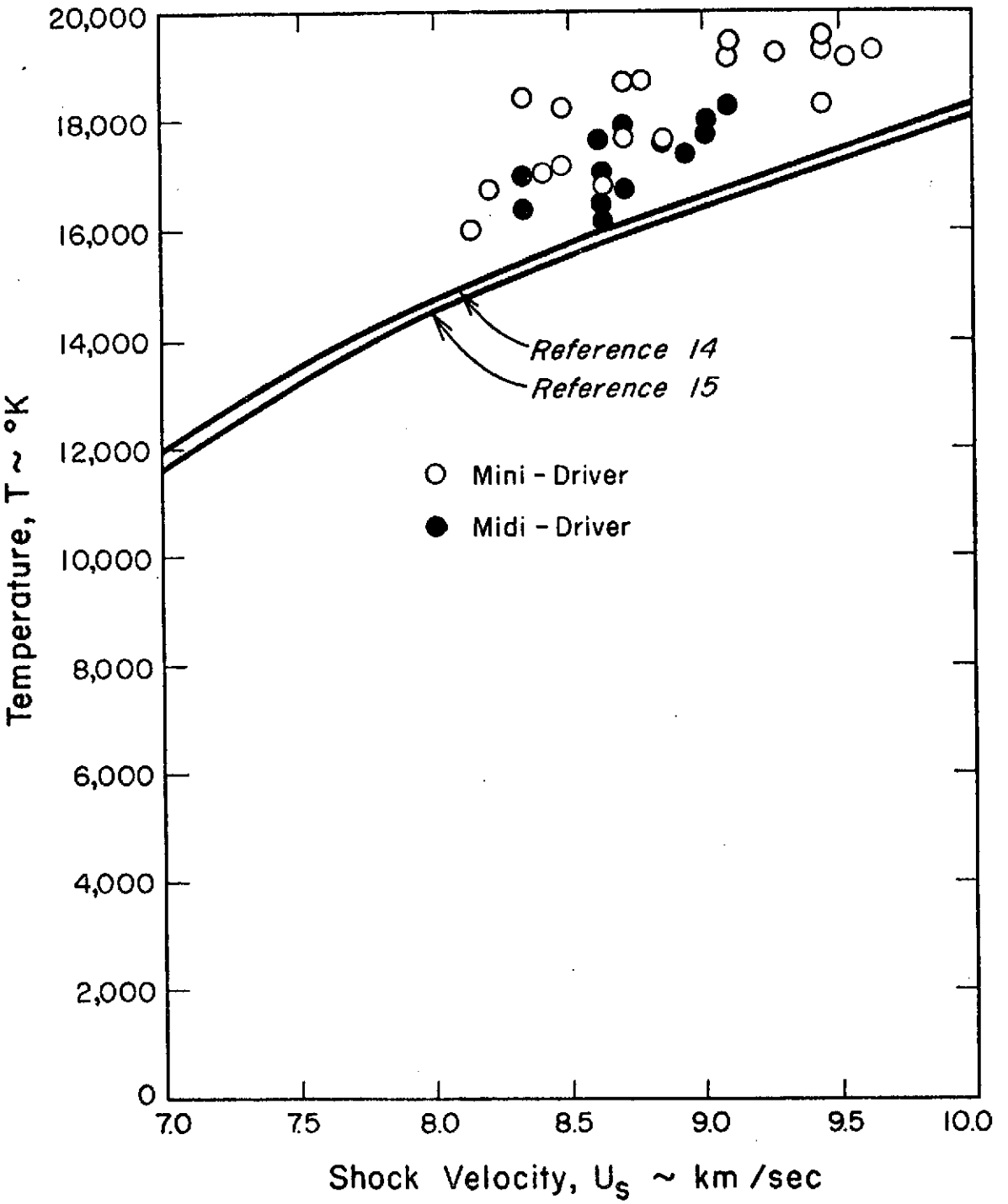

Fig. 19. Comparison of DAIM Temperature Measurements at t = 1 μs After Shock Passage, P_1 = 1 torr, x = 3.6 mm, and for Mini-Volume and Midi-Volume Drivers

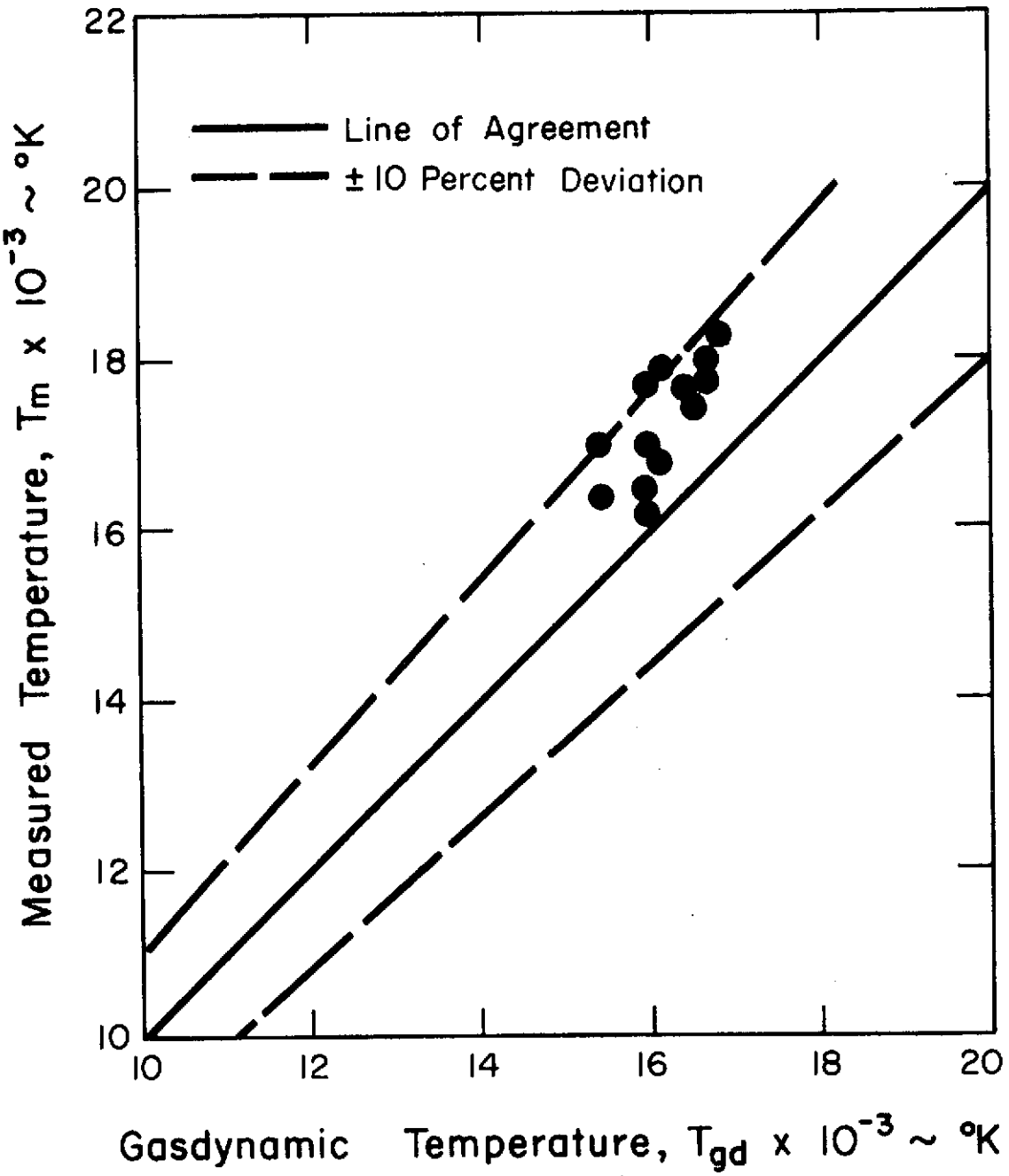

Fig. 20. Measured DAIM Temperature Versus Predicted Gas Dynamic Temperature from Reference 13, t = 1 μs After Shock Passage, P_1 = 1 torr, x = 3.6 mm, Midi-Volume Driver Used

than acceptable and the deviation shown in Figs. 14 and 20 would not be of concern. However, we felt that we could make a more accurate temperature measurement using DAIM and we believe that, in fact, we have, i.e., much of the difference between the data and the predictions is felt to be real and not due to experimental error or technique.

This conclusion does not mean that the DAIM technique cannot be improved upon. From an experimental viewpoint, there are many things that can be done; for example, by using a single beam oscilloscope, a full 10 cm of deflection would be available. Camera techniques could be improved. A more accurate method for reading calibration current could be employed. A calibration lamp directly from NBS could be employed, and better control of lamp filament current would be of benefit. Finally, and very importantly, an improved signal-to-noise ratio would lead to improved accuracy. This could be done, as an example, by viewing a larger volume of gas or by using interference filters instead of monochromators for wavelength resolution.

In closing, it should be noted that there are several possible optical path arrangements to use in making the DAIM type measurement. The simplest arrangement is to place a splitter in the shock tube and divide the tube width unequally. Then the radiation may be observed from the two different slab thicknesses as is illustrated in Fig. 21(a). Ideally, of course, the splitter should be a perfect absorber with no reflections occurring off its surface (since the splitter surface will not attain a very high temperature during the test time, any surface emission should be negligible). For a given shock-tube size, the geometry of Fig. 21(a) does not give the largest τ_1 values possible, thus forcing the opacity to lower values and degrading the accuracy of the measurement. However, by either placing a hole in the splitter, viewing at right angles (see Fig. 21(b)), or off-setting one beam as is illustrated in Fig. 21(c) and as was done here, the longest path ℓ_1, can be made to be the shock-tube diameter. Again, this technique requires that the far viewing wall reflections on each channel be zero.

An alternative to using a splitter is to make the far wall highly reflective on one channel so that the optical depth of that path can be doubled to 2d. This configuration, illustrated in Fig. 21(d), would have the advantage of keeping the optical paths at least as good as those for a straight brightness measurement. The main problem here would be in making the far wall a perfect reflector. A mirrored surface in contact with the flow is questionable because of both surface quality and possible alignment problems. A mirror located behind a window may be acceptable, and, in this case, the finite transmission of the window for two passes through it and the finite reflectivity of the mirror must be taken into account in data reduction and interpretation. The spatial resolution will also be degraded due to the increased path length, but this could possibly be overcome by using a focusing mirror instead of a flat mirror. Obviously, there are other possible optical path arrangements as well. Each of these would have to be

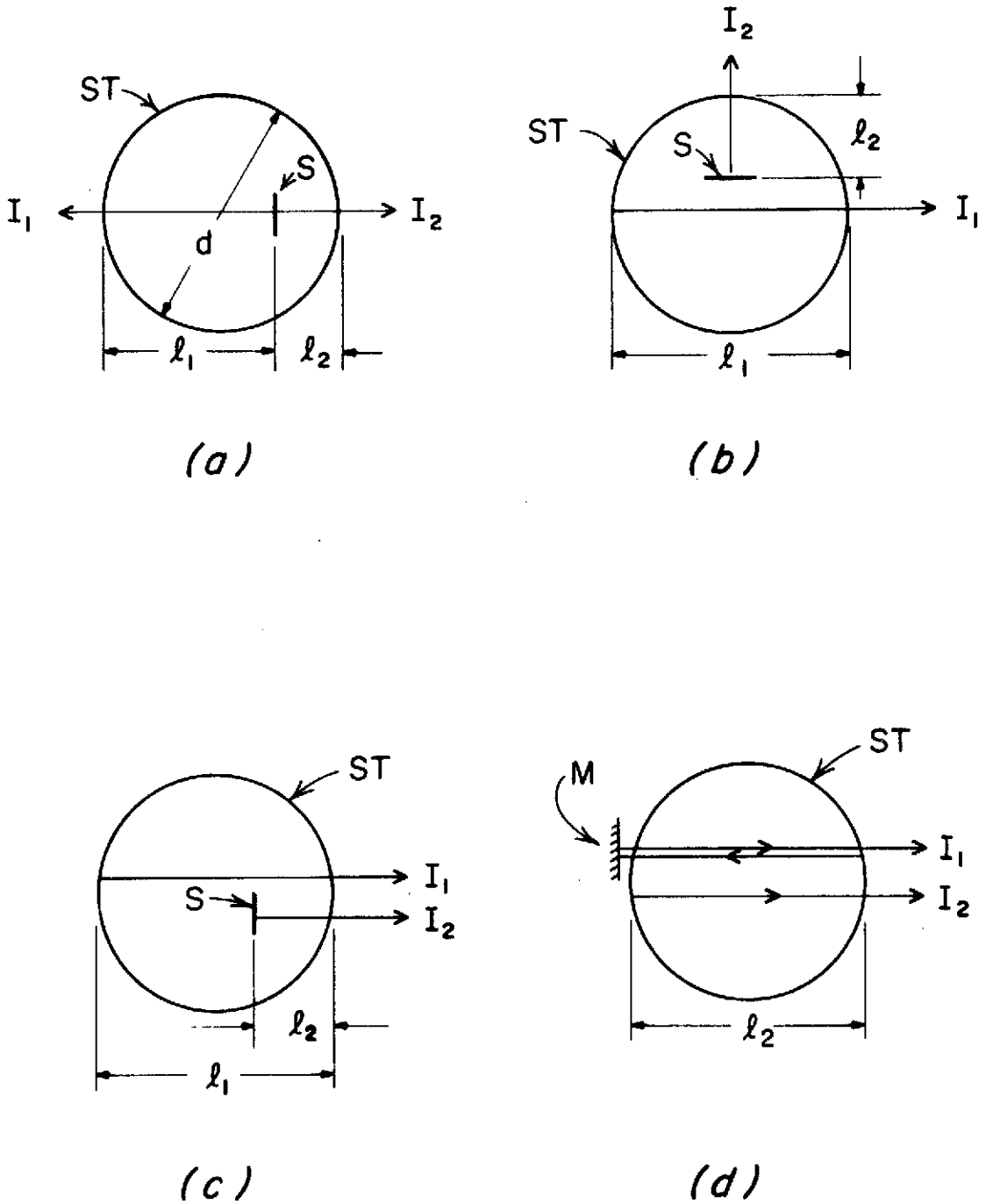

Fig. 21. Possible Optical Path Arrangements for Application of DAIM Technique (ST-shock tube, S-splitter, M-mirror)

considered on its own merits and in terms of the facility on which it is to be applied.

VI. CONCLUSIONS

It is believed that the results of this investigation have shown the Double Absolute Intensity Measurement, or DAIM, technique to be a useful diagnostic tool in gas dynamic studies.

The difference between the measured temperatures and the predicted gas dynamic values which were found in the present experiments is felt to be in no way an indictment of the technique. Rather, the technique has, if anything, proved useful in pointing out certain apparent facility related problems. As can be seen in Figs. 14 and 20, the data scatters only by approximately ± 5 percent around its own mean. This is consistent with the error analysis, and it is felt that this could be improved.

It should be noted that one of the advantages of DAIM is that it provides a measurement of both temperature and optical thickness. On the basis of the latter, one can then determine whether or not the data obtained are in an appropriate optical thickness range for the DAIM measurement to be sufficiently accurate and to be representative of the gas conditions.

In addition, there are a variety of path length arrangements which can be used in carrying out DAIM measurements. Certain questions, however, are still unanswered and need to be investigated further. These include those pertaining to the effects of boundary layers and of spectral variations over the wavelength interval to be used.

REFERENCES

1. Wood, A. D. and Wilson, K. H., "Radiant Energy Transfer Measurements in Air," NASA CR-1390, Washington, D.C., 1969.

2. Wood, A. D. and Wilson, K. H., "Thermodynamic Property Measurements in Reflected Shock Air Plasmas at 12-16,000°K," NASA CR-1617, Washington, D. C., 1970.

3. Bengston, R. D. Miller, M. H., Koopman, D. W., and Wilkerson, T. D., "Comparison of Measured and Predicted Conditions Behind a Reflected Shock," Phys. Fluids, Vol. 13, No. 2., February 1970, pp. 372-377.

4. Griem, H. R., Plasma Spectroscopy, McGraw-Hill Book Co., New York, 1964.

5. Soloukin, R. I., "Shock Tube Diagnostics, Instrumentation, and Fundamental Data," Shock Tubes, Proceedings of the Seventh International Shock Tube Symposium, ed. I. I. Glass, University of Toronto Press, 1970, pp. 662-706.

6. Nerem, R. M., Golobic, R. A., and Bader, J. B., "Laboratory Studies of Radiative Transfer Effects in Shock-Heated Gases," Shock Tube Research, Proceedings of the Eighth International Shock Tube Symposium, July 5-8, 1971, Chapman and Hall, London, pp. 19/1-19/19.

7. Morris, J. C., "The Continuum Radiation of Oxygen and Nitrogen for Use in Plasma Temperature Determination," J. Quant. Spec. Rad. Trans., Vol. 6, No. 6, Nov-Dec. 1966, pp. 727-740.

8. Bader, J. B., "The Development of a Brightness Temperature Measurement Technique for Application to Shock Tube Produced Flows," M.Sc. Thesis, Department of Aeronautical and Astronautical Engineering, The Ohio State University, 1971.

9. Golobic, R. A.,"Laboratory Studies of Strong Shock Waves in Xenon," Ph.D. Dissertation, Department of Aeronautical and Astronautical Engineering, The Ohio State University, 1971.

10. Lee, J. D., and Nerem, R. M., "Test Duration Measurements in a Shock Tube Having an Arc-Heated Driver," The Ohio State University Lab Report No. 1021-18, June 15, 1962.

11. Graber, B., and Nerem, R. M., "Test Duration Measurements in an Arc-Driven Hypervelocity Shock Tube," The Ohio State University, Aerodynamic Laboratory Report No. 1573-2, October 1963.

12. Menard, Wesley A., and Thomas, George M., "Radiation Measurement Techniques," Jet Propulsion Laboratory Technical Report No. 32-975, 1966.

13. Golobic, R. A. and Nerem, R. M., "Shock Tube Measurements of End-Wall Radiative Heat Transfer in Air," AIAA Journal, Vol. 6, No. 9, Sept. 1968, pp. 1741-1746.

14. Menard, W. A. and Horton, T. E., "Shock-Tube Thermochemistry Tables for High Temperature Gases. Vol. 1: Air," Jet Propulsion Laboratory (NASA) Technical Report 32-1408, Pasadena, California, 1969.

15. Laird, J. D. and Heron, K., "Shock Tube Gasdynamic Charts. Part I: Equilibrium Argon-Free Air from 3,000 to 40,000°K," Avco-RAD TM 64-12, April 10, 1964.

16. Nerem, R. M., Carlson, L. A., and Golobic, R. A., "Radiation-Gasdynamic Coupling Behind Reflected Shock Waves in Air," presented at the 12th International Congress on Applied Mechanics, Stanford University, California, August 26-31, 1968.

17. Nerem, R. M., "Research on Problems of High Enthalpy Flows," Aerospace Research Laboratories Report ARL 69-0145, September 1969.

18. Knott, P. R., Carlson, L. A., and Nerem, R. M., "A Further Note on Shock Tube Measurements of End-Wall Radiative Heat Transfer in Air," AIAA Journal, Vol. 7, No. 11, Nov. 1969, pp. 2170-2172.

19. Nerem, R. M., Carlson, L. A., and Hartsel, J. E., "Chemical Relaxation Phenomena Behind Normal Shock Waves in a Dissociated Free-stream," AIAA Journal, Vol. 5, No. 5, May 1967, pp. 910-916.

20. Nerem, R. M., "Radiative Transfer Effects Behind Reflected Shock Waves," Ohio State University Research Foundation Final Report on NASA Grant NGL-36-008-106, March 1972.

21. Strehlow, R. A., and Cohen, A., "Limitations of the Reflected Shock Technique for Studying Fast Chemical Reactions and Its Application to the Observation of Relaxation in Nitrogen and Oxygen," J. Chem. Physics, Vol. 30, No. 1, 1959, pp. 257-265.

22. Dyner, H. B., "Density Variation Due to Reflected Shock Boundary Layer Interaction," Phys. Fluids, Vol. 9, No. 5, 1966, pp. 879-892.

23. Mirels, H., "Boundary Layer Growth Effects in Shock Tubes," Shock Tube Research, Proceedings of the Eighth International Shock Tube Symposium July 5-8, 1971, ed. J. L. Stollery, Chapman and Hall, London, pp. 6/1-6/30.

24. Mirels, H., "Test Time in Low-Pressure Shock Tubes," Phys. Fluids, Vol. 6, No. 9, September 1963, pp. 1201-1214.

25. Yoshinaga, T., "Time-Resolved Spectroscopic Measurements Behind Incident and Reflected Shock Waves in Air and Xenon," M. Sc. Thesis, Department of Aeronautical and Astronautical Engineering, The Ohio State University, 1972.